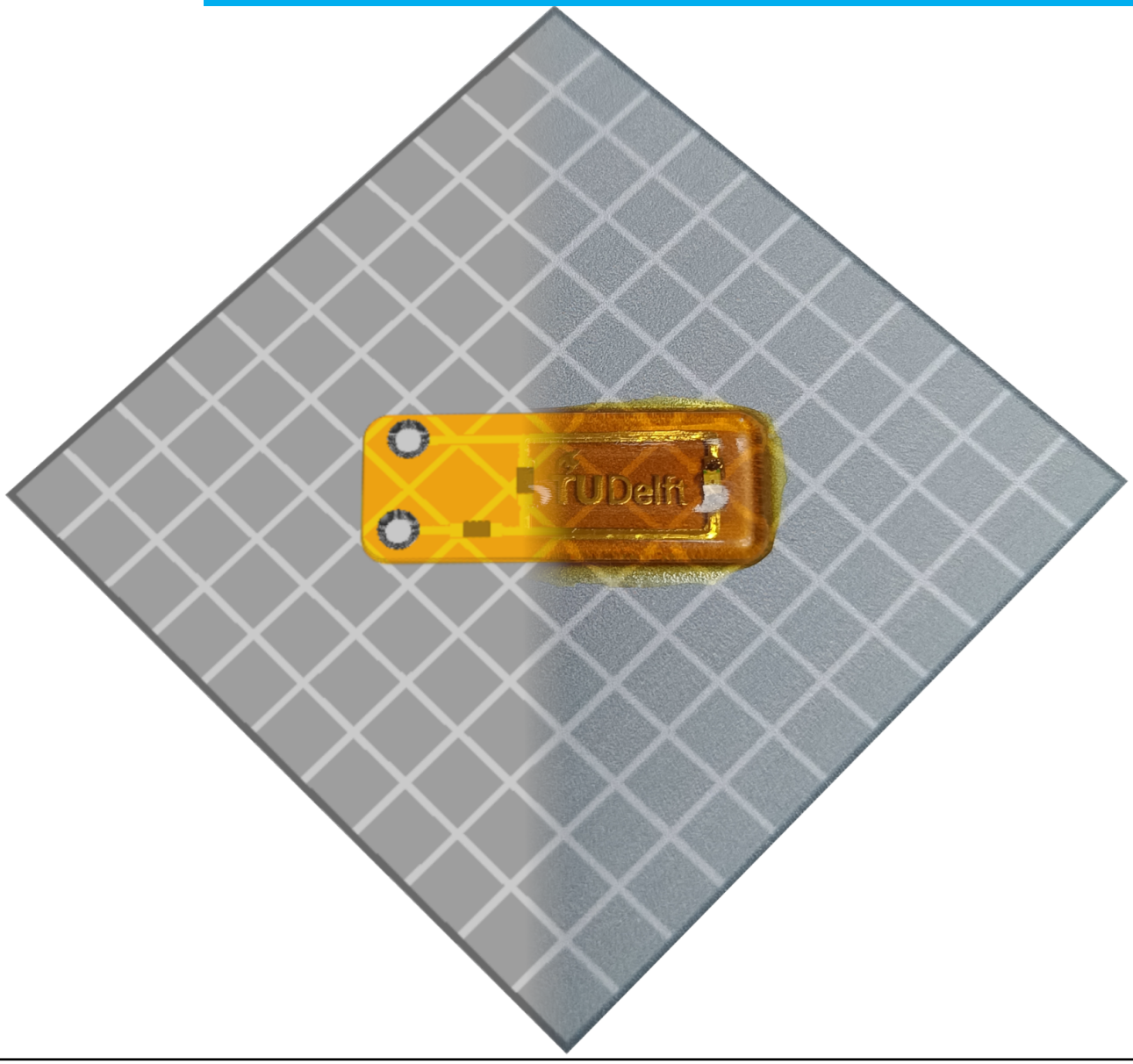
Department of Precision and Microsystems Engineering

Inkjet-3D-printing of structural electronics: Development of a 3D slicer and experimental testing

Martijn den Hoed

Report no : 2025.030
Professor : Dr. Ir. J.F.L. Goosen
Specialisation : High-Tech engineering
Type of report : Master Thesis
Date : 11-07-2025



TU Delft Delft University of Technology

Challenge the future

Preface

This thesis represents the conclusion of the five years that I spent at the TU Delft. It is a combination of the many things I've learned during my studies, which range from the basics of engineering to more niche topics such as micro-fabrication and additive manufacturing. Additionally, I was able to incorporate several personal interests, such as voxel-based algorithms, rendering techniques, and electronics design. I'm very proud of the results that I have achieved in this thesis, and hope that the techniques and concepts that are discussed in this report may aid or inspire future research in this topic.

I would like to thank my supervisor, Hans Goosen, for guiding me through this thesis and giving me the freedom to explore the aspects of this topic that I found most interesting. Next, I'd like to thank Andres Hunt and Giuolio Gallucci for sharing their experience in inkjet-printing and helping me use the Pixdro LP50.
Finally, I would like to thank my friends and family for their support throughout my studies.

Martijn den Hoed
Delft, July 2025

Abstract

Additive manufacturing is a highly transformative technology. The ability to fabricate a physical component solely from digital designs offers many unique advantages that are not seen in conventional manufacturing techniques. One of these additive manufacturing processes, inkjet-3D-printing, has the capability to accurately construct 3D shapes while offering the option to utilize multiple different materials.
By making use of specialty inks, such as conductive inks and photopolymer inks, it becomes feasible to construct embedded electronic circuits in 3D solids, a concept referred to as structural electronics.
Several aspects of this process remain challenging, however: there is a wide variety of printable photopolymers, each with different printing requirements and material characteristics. Likewise, although conductive inks are commercially available, many formulations require intense post-processing or offer limited conductivity. Furthermore, there is an absence of open software tools dedicated to the design and integration of structural electronics for inkjet-3D-printing.
In this thesis, the use of a TPGDA photopolymer in combination with a silver nanoparticle ink is investigated for the application of printing structural electronics. The materials are printed using a PIXDRO LP50 Inkjet printing platform equipped with Dimatix printheads. The TPGDA is cured with UV light, which results in accurate, millimeter-scale structures, although artifacts are present due to fluid interactions of the liquid photopolymer.
The silver nanoparticle ink, NovaCentrix Metallon JS-A211, is printed on the polymer substrate and sintered with intense UV light, a process known as photonic sintering. Circuit traces are consistently printable with a minimum width of 0.3 mm, and a sheet resistance of 0.21Ω per layer has been achieved.
To support the fabrication process, a software tool is developed for pre-processing files for inkjet-3D-printing, and for designing and embedding electronic circuits. This tool is used to design a series of print tests, where the structural and conductive materials are combined to form structural electronics. In these print tests, the ability to incorporate electronic vias into the printed circuit is demonstrated. Additionally, electronic components are successfully soldered to the fabricated designs, and the ability to embed these components into the structural material is achieved.

Contents

Preface i

Summary ii

Nomenclature v

1 Introduction 1
- 1.1 Research subject . . . 2
- 1.2 Report outline . . . 2

2 State of the art 3
- 2.1 Overview of Inkjet printing . . . 3
  - 2.1.1 Continuous-Inkjet . . . 3
  - 2.1.2 Drop-On-Demand . . . 3
  - 2.1.3 Droplet formation . . . 4
  - 2.1.4 Substrate interactions . . . 5
  - 2.1.5 Specialty inks . . . 6
  - 2.1.6 PolyJet and MultiJet process . . . 6
- 2.2 Inkjet printing of electronic structures . . . 7
  - 2.2.1 Structural inks . . . 7
  - 2.2.2 Conductive inks . . . 8
  - 2.2.3 Sacrificial material . . . 9
  - 2.2.4 Material compatibility . . . 9
  - 2.2.5 Printing of circuit building-blocks . . . 10
- 2.3 Model preparation software . . . 11
  - 2.3.1 3D-printer slicer functionality . . . 11
  - 2.3.2 Slicers in inkjet-3D-printing . . . 11
  - 2.3.3 Electronics integration . . . 12

3 Printing setup 13
- 3.1 Pixdro LP50 . . . 13
- 3.2 Printhead . . . 13
- 3.3 Pixdro HMI . . . 14
- 3.4 Modifications for 3D-printing . . . 15

4 Model preparation software 16
- 4.1 Slicer requirements . . . 16
- 4.2 Slicer implementation . . . 17
  - 4.2.1 Structural material slicing . . . 17
  - 4.2.2 GUI . . . 18
  - 4.2.3 Support generation . . . 19
  - 4.2.4 Circuit designing . . . 20
  - 4.2.5 Circuit vertical segmenting . . . 21
  - 4.2.6 Non-planar embedded circuits . . . 21
  - 4.2.7 Via generation . . . 22
  - 4.2.8 Component importing and slicing . . . 24
  - 4.2.9 Layer rendering & exporting . . . 24

5 Polymer inkjet printing 25
- 5.1 Ink selection . . . 25
- 5.2 Ink preparation . . . 25
- 5.3 Jetting parameters . . . 25

5.4 Print parameters . . . 26
5.4.1 DPI, Step Size & Quality Factor . . . 26
5.4.2 UV curing . . . 28
5.4.3 Print acceleration . . . 28
5.4.4 Substrate . . . 28
5.5 Results . . . 29
5.5.1 Ramp test . . . 29
5.5.2 Line test . . . 30
5.5.3 Aspect ratio test . . . 31
5.5.4 Design rules . . . 32

6 Conductor inkjet printing 33
6.1 Ink selection . . . 33
6.2 Jetting parameters . . . 33
6.3 Process parameters . . . 34
6.3.1 Quality factor & step size . . . 34
6.3.2 Sintering parameters . . . 34
6.3.3 DPI calibration . . . 35
6.3.4 Substrate treatment . . . 35
6.4 Print Results . . . 36
6.4.1 Resolution test . . . 36
6.4.2 Conductivity . . . 38

7 Structural electronics printing 39
7.1 Software Workflow . . . 39
7.2 Printing workflow . . . 40
7.3 Results . . . 40
7.3.1 Circuit overprinting . . . 41
7.3.2 Via test . . . 41
7.3.3 Component bonding . . . 42
7.3.4 Component Embedding . . . 43
7.3.5 Printing exposed pads . . . 45

8 Discussion 46
8.1 Slicer . . . 46
8.2 Polymer printing . . . 46
8.3 AGNP printing . . . 47
8.4 Structural electronics printing . . . 47

9 Recommendations 48

10 Conclusion 50

References 52

A Slicer main program loop 55

B Slicer documentation 58

C LP50 printing profile 63

D Additional test-prints 65

Nomenclature

Abbreviations

Abbreviation	Definition
AGNP	Silver Nanoparticle
CAD	Computer Aided Design
CIJ	Continuous-Inkjet
DIW	Direct Ink Writing
DLP	Digital Light Processing
DPI	Dots Per Inch
DOD	Drop On Demand
FDM	Fused Deposition Modelling
FFF	Fused Filament Fabrication
GUI	Graphical User Interface
HDT	Heat Deflection Temperature
HMI	Human Machine Interface
HPB	Head Personality Box
PCB	Printed Circuit Board
PCBA	Printed Circuit Board Assembly
PHA	Print Head Assembly
P&P	Pick and Place
QF	Quality Factor
SMD	Surface Mount Device
SLA	Stereo Litography Apparatus
SLS	Selective Laser Sintering
SS	Step Size
TGME	Triethylene Glycol Methyl Ether
TOF	Time Of Flight
TPGDA	Tripropylene Glycol Diacrylate
UV	Ultra Violet

1

Introduction

The emergence of additive manufacturing, commonly known as 3D-printing, has transformed various fields of engineering by enabling the fabrication of physical components from a mere digital design with minimal manual intervention.
In the field of mechanical engineering, 3D-printing enables rapid prototyping and decentralization of production, reducing the time from concept to a tangible object to hours. In addition to prototyping purposes, this class of technologies enables the creation of intricate geometries beyond the constraints of conventional manufacturing techniques, resulting in designs that are lighter, more optimized, and more capable.

In the field of circuit board fabrication, a development of this nature has not yet occurred. For over seven decades, electronic circuits have been predominantly produced in centralized facilities using traditional photolithography methods, a process that remains largely unchanged today [47]. However, recent global events have underscored the value of decentralized manufacturing approaches, which not only enhance rapid R&D capabilities but also offer improved control over intellectual property and secure supply chains.

In recent years, progress in multi-material 3D printing technologies has opened doors for the additive manufacturing of functional electronic circuits. This breakthrough includes a range of systems and platforms, from commercial machines to innovative research platforms capable of printing conductive materials alongside structural materials. While early research-systems were predominantly limited to extrusion-based printing methods, innovations and commercialization in the field of photopolymers and nanoparticles have introduced the ability to utilize Inkjet-printing for producing both structural and conductive materials in a single process.

This advancement in Inkjet-based 3D printing signifies a pivotal development: it is now feasible to use a single machine to fabricate high-resolution electronic circuits embedded into traditionally mechanical components. This concept, where components serve both a structural function and an electronic function, is known as structural electronics. This emerging field has a broad range of possible applications, such as embedding biomimetic, nerve-like structures into aircraft skin for enhanced sensing, or printing OLED displays directly onto automobile panels. [46] Additional opportunities for this fabrication process lie in additive manufacturing of semiconductor packaging [25], and rapid prototyping of PCBs. [15]

1.1. Research subject

Although the process of inkjet printing electronic circuits has been the subject of extensive academic research, the majority of these studies primarily focus on printing single-layer circuits on flat substrates. For the purpose of inkjet-3D-printing structural electronics, which refers to electronic circuits embedded in mechanical components, there are still many aspects that are relatively poorly explored. These include finding an Inkjet-printable structural material that can withstand high temperatures, a conductor that is compatible with such a structural material while retaining good conductivity, and methods for bonding electronic components to the printed structures to enable the fabrication of fully functional circuits.

Apart from material challenges, a major contributor to the usability of 3D-printing technologies is the availability of robust software tools for designing 3D models and processing them for additive manufacturing. Again, this area has received relatively little academic attention in the field of inkjet-3D-printing and especially in the field of printing structural electronics.

This report aims to address both these gaps in the literature by seeking to fulfill the following research goal:

Develop a 3D slicer for Inkjet-3D-printing structural electronics, and experimentally validate this through multimaterial Inkjet printing.

1.2. Report outline

In this report, firstly the prior literature on this topic is explored in chapter 2, where the concepts behind Inkjet-printing are explained, the application of Inkjet for 3D printing structural electronics is investigated, and the principles behind model preparation software and slicers are discussed.

Next, in chapter 3 the printing platform and hardware that have been used in this report are explained. chapter 4 describes the development of a slicer program which can process 3D models into a format that can be Inkjet-3D-printed, and contains algorithms for designing and integrating electronic circuits into these models. In chapter 5, the settings and parameters for printing the structural material are tuned, and the results of the printed models are analyzed. This same process is repeated in chapter 6, but instead focuses on printing a conductive material. In chapter 7, the structural and conductive material are combined to print structural electronics. Several print-tests are performed, and the results and challenges are analyzed.

The findings from this research are discussed in chapter 8, and several recommendations are made both to aid future research and to inspire new research topics in chapter 9.

Finally, in chapter 10, the report is summarized and concluded.

2

State of the art

In this chapter, an overview is provided of the process of inkjet-3D-printing and developments in the state of the art. section 2.1 describes the working principles of inkjet printing and how this technology is applied to facilitate 3D printing. In section 2.2, inkjet-3D-printing of electronic structures is explored, including an overview of inks and materials that have been used in prior literature.
Finally, in section 2.3 the software tools and functionalities required for additive manufacturing are investigated, and an overview is given of software developments in the field of 3D-printing structural electronics.

2.1. Overview of Inkjet printing

Inkjet printing is widely recognized for its application in consumer-grade 2D printers, where it is employed to deposit various colored inks to produce full-color images. In addition to this well-known use, Inkjet printing has a broad range of industrial applications, including printing expiration dates on products, creating colorful patterns on textiles, and printing RFID antennas.

Several techniques have been developed for Inkjet printing, with the most prevalent being Drop-On-Demand (DOD) and Continuous Inkjet (CIJ) printing systems. [16]

2.1.1. Continuous-Inkjet

In Continuous-Inkjet printing, a continuous stream of ink droplets is expelled from a pressure-fed nozzle. These droplets fall between a set of charged plates, which, through electrostatic repulsion and attraction, guide the droplets either into a collection bin or onto the substrate. This technique is most commonly applied in high-throughput industrial processes, where printing quality is not of high importance, such as the printing of expiration dates on products. Downsides of this process include: [53]

- Inks may get contaminated during printing due to the fact that the ink is recycled after falling into the collection bin.
- The inks have to be electrically conductive since they rely on electrostatic repulsion and attraction for their operation.
- The viscosity of the inks has to be relatively low to allow correct droplet formation, limiting the range of viable inks.

2.1.2. Drop-On-Demand

Drop-On-Demand (DOD) Inkjet printing is the technique well-known for its use in consumer-grade Inkjet printers. In contrast to CIJ printing, DOD has the ability to dispense individual ink droplets, without the need for a continuous stream of droplets. Again, this technology can be further subdivided into different classes, the two most prevalent being: Thermal Inkjet printing and Piezo Inkjet printing.

In thermal Inkjet printing, a electric heating element is positioned inside the ink reservoir, which can be

rapidly heated. This heating creates a vapor bubble with enough pressure to expel a small amount of ink through the nozzle attached to the ink reservoir.
Individual droplets of ink can be precisely deposited this way, but the thermal heating does put limitations on the assortment of available inks; The inks must be able to withstand the elevated temperatures without significant degradation, but must also create a sufficiently large vapor bubble when heated. [16]

In Piezo Inkjet printing, a similar concept is applied, but instead of a vapor bubble, a piezo element is used to displace the ink in the ink reservoir, thereby expelling a droplet.
An advantage of this technique is that more accurate control of the pressure on the ink is possible, and a wider variety of inks can be used, as the inks are not exposed to high temperatures. [16]

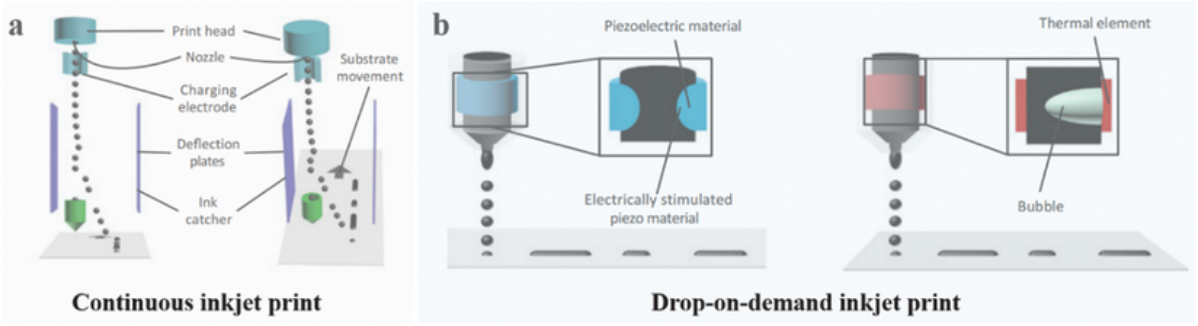


Figure 2.1: Depiction of Continuous Inkjet printing (a), Drop On Demand Inkjet printing (b). Adapted from [21]

2.1.3. Droplet formation

In an ideal scenario, the expelled ink forms a single droplet, and remains in that form until it reaches the substrate. Other scenarios also occur however, such as when smaller, 'satellite' droplets are formed behind the main droplet, which negatively impacts the quality of the print.
Several physical parameters influence this phenomenon, those being the ink's viscosity, velocity, density, and surface tension. These parameters are often combined into a single dimensionless parameter, known as the Z-value, or the reciprocal of the Ohnesorge number, shown in Equation 2.1.

$$Z = \frac{1}{\mathrm{Oh}} = \frac{\sqrt{\rho\sigma a}}{\mu} = \frac{\mathrm{Re}}{\sqrt{\mathrm{We}}} \tag{2.1}$$

Where μ is the ink's dynamic viscosity, ρ the density, σ the surface tension, and a the droplet diameter. Alternatively, the Z-value can be described as the ratio between the Reynolds number and the square of the Weber number, where the Reyonolds number relates the liquid's inertial and viscous forces, and the Weber number the inertial and surface tension forces.
Ink formulations with a Z-number lying between 1 and 10 are considered to be jettable, where lower values indicate that the ink is too viscous to be expelled, and higher values indicate the ink is not viscous enough, resulting in the formation of satellite droplets.[3]

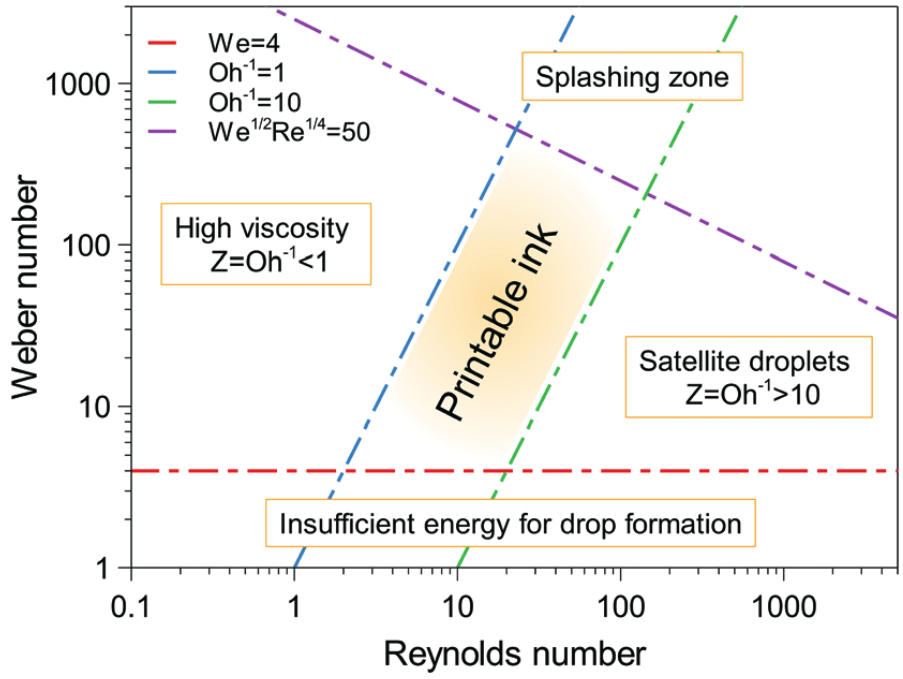


Figure 2.2: Jettability of liquids based on the Reynolds and Weber numbers, adapted from [24]

2.1.4. Substrate interactions

When the droplet has reached the substrate, several factors, including the wettability, determine how the deposited liquid spreads. Low wettability indicates a large contact angle and can result in beading of the deposited droplets, preventing the formation of thin layers.
High wettability indicates a small contact angle, resulting in good adhesion between the substrate and the deposited material.
Inkjet inks are typically water- or alcohol-based, meaning that they have good wettability on hydrophilic surfaces, and the opposite for hydrophobic surfaces. This property of the surface material can be adjusted using a variety of surface treatments, such as adding fluorocarbon coatings, UV irradiation, and plasma treatment. [33]
After making contact with the substrate, the deposited liquid will take on the temperature of the substrate, which, depending on the type of ink, can be cooled or heated. Inks based on molten polymers or metals are typically printed on ambient or cooled substrates, causing droplets to cool and solidify after deposition.
Other inks utilize evaporation of a solvent, or elevated temperatures for polymerization, and therefore rely on the substrate being heated.[16]

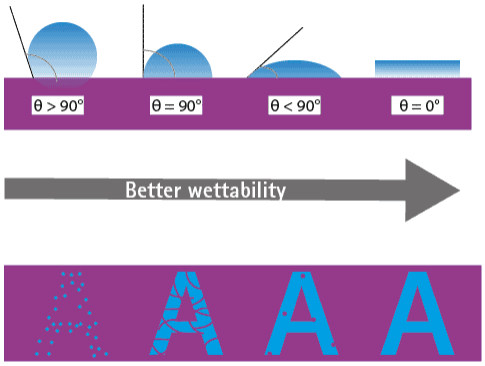


Figure 2.3: Effects of wettability on the droplet contact angle and quality of the print, adapted from [35]

2.1.5. Specialty inks

Inkjet technology has been applied far beyond the printing of just water-based inks. Coloured UV curable resins, used by digital flatbed printers, are commonly used for printing on less conventional surfaces, such woods, glasses and a variety of plastics. [52]
This same principle of selectively depositing photopolymers has been applied for printing structural parts, where several layers of UV curable resins are deposited and cured on top of each other, resulting in 3D-dimensional, polymer-based structures. This process has been developed into one of the most prominent 3D-printing technologies, trademarked under the names PolyJet and MultiJet. [34]
Other materials printable using techniques similar to the Inkjet process include thermoplastic polymers and low-melting-point metals. Here, the feedstock is loaded into the printhead in a solid state, where it is melted and selectively deposited through the nozzle by means of piezo actuators, electrostatic fields, or pneumatic pressure pulses. [19] [12]
Finally, nanoparticle suspensions are printable with Inkjet technology and are a way to print materials with properties more favourable than those of pure polymers. Metal nanoparticle suspensions can result in highly conductive patterns after a sintering step, and ceramic nanoparticle suspensions can polymerize into composite materials with superior mechanical behavior. [3]

2.1.6. PolyJet and MultiJet process

Derived from the principles of Inkjet printing is the process of Polyjet and MultiJet printing, a process originally developed in the 1990s, and currently trademarked by the companies Stratasys and 3D Systems respectively. [32]
The process uses exclusively piezo-based printheads and dispenses a variety of UV-curable resins from an array of nozzles. These resins can have varying colours and mechanical properties, and gel-like resins can be used as soluble support material, allowing the printing of overhanging structures.
These materials are deposited in 2-dimensional patterns, which are successively stacked to form 3-dimensional shapes. To ensure flatness of the printed layers, a blade [32] or roller [48] is deployed, which either removes excessive material or flattens material that exceeds the desired layer height. After this step, the UV-light source integrated in the printhead, irradiates and cures the newly deposited layer, thereby solidifying it.
Variations in this order exist, where the deposited droplets are directly exposed to mild UV-light, to slightly cure it into a gel-like state, before being flattened and fully cured. This procedure, called 'pinning', can enhance the achievable resolution, but is highly dependent on the curing energy applied in the initial curing. [9]

Normally, a glossy surface finish is present on surfaces where no support material was applied, and a matte finish where support material was present. For a uniform surface finish, a thin coating of support material can be printed surrounding the entire surface of the model, ensuring a uniform matte finish. [7]

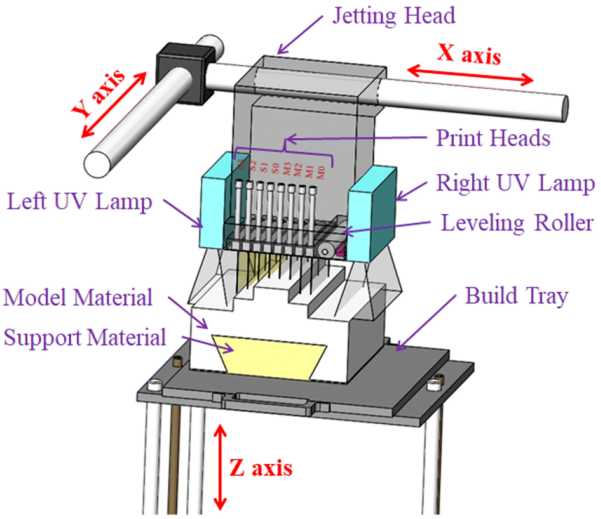


Figure 2.4: Depiction of the motion system and printhead assembly of the Polyjet printing process, showing the Inkjet nozzles, UV lamps, and levelling roller. Adapted from [36]

2.2. Inkjet printing of electronic structures

In recent developments, the multi-material capability of Inkjet printing has been exploited for printing electronic structures. To achieve this, a structural and a conductive material must be available. In order to form true 3-dimensional shapes, an additional, sacrificial material is required to support areas where an overhang would otherwise be present. Several different combinations of materials have been demonstrated in literature, and are discussed in the following sections.

2.2.1. Structural inks

Structural material for the purpose of Inkjet-printed electronics has been mostly limited to UV-curable ink. Commercially available materials, such as the Stratasys Vero material, have been applied in this context [6], and are available in a variety of colors. Furthermore, variations with more favorable mechanical and temperature properties have been developed, such as Durus and Rigus, allowing the printed parts to have functions beyond just aesthetic purposes. [34]
A potential downside of these materials is their proprietary nature, as their exact composition is not disclosed.

Custom structural Inkjet materials have been documented in academic research, consisting of a mix of isomers and photoinitiators, which polymerize when exposed to a UV light source. [14]
Nanoparticle suspensions of silicon oxide have also been used as a substrate for printed electronics; After polymerization, this effectively forms a composite material with potentially superior mechanical properties than those of pure polymers. [20]

Table 2.1: Collection of commercially available photopolymer inks for 3D-Inkjet-printing

Name	Brand	Remarks	Relevant Publications
Vero [34]	Stratasys	Proprietary 47$^{\circ}C$ HDT	[6]
High Temperature [34]	Stratasys	Proprietary 65$^{\circ}C$ HDT	
VisiJet M2S-HT250 [49]	3D Systems	Proprietary 250$^{\circ}C$ HDT	
Dielectric ink 1092 [30]	Nano Dimensions	Proprietary Known to work with sintering of AGNP ink	
TPGDA	-	Known composition Known to work with sintering of AGNP ink Modifyable for support material	[39] [14]
mr-UVCur26SF [29]	Microresist	Proprietary Typically used for nano-imprint lithography	
InkOrmo [18]	Microresist	Proprietary Typically used for optical structures Clear to visible light	[22]
Sunjet line [8]	DIC/SunChemical	Proprietary Acrylate-based	[37]

2.2.2. Conductive inks

The Inkjet printing of conductive materials is commonly performed using nanoparticle inks. These inks contain nano-scale particles of metal suspended in a liquid, often water- or alcohol-based.
Additionally, they can contain additives such as surfactants to improve wetting behavior on hydrophobic surfaces.
After deposition, the ink dries but does not yet become conductive; a sintering step is required for this. Four types of sintering are typically applied for nanoparticle inks:

- Thermal sintering: The entire substrate is evenly heated until the sintering temperature is reached.
- Infrared photonic sintering: High intensity infrared light is applied to irradiate and heat the nanoparticles such that sintering occurs.
- UV photoinic sintering: Ultra-Violet light is applied to irradiate and heat the nanoparticles such that sintering occurs.
- Chemical sintering: The nanoparticle ink is printed on a pre-treated substrate, containing additives that induce sintering of the nanoparticles.

Silver, being the most conductive metal, has been widely used for this purpose due to its high conductivity and low oxidation rate. Furthermore, the sintering temperature of silver is significantly lower than that of other metals used for nanoparticle suspensions. Additionally, silver nanoparticles with a size smaller than 50nm have a peak in the absorption spectrum near 400nm, making UV light an effective tool for photonic sintering. [39] Other metals have been used in nanoparticle inks as well, mainly gold and copper, but are less advantageous due to their high cost and high oxidation rate, respectively. [3]

Carbon black inks and conductive polymers have been applied for printing electrodes and traces as well, but due to their resistivity being orders of magnitude higher than that of metals, their use-case is often limited to applications such as resistive components and sensors. [23]

Table 2.2: Collection of commercially available silver-nanoparticle inks

Name	Brand	Base	Nanoparticle wt%	Remarks	Relevant Publications
Metalon JS-A series [17]	Novacentrix	Water	30-40%	Sinterable with UV-light	[6]
Metalon JS-B series [17]	Novacentrix	Water	25%	Sinterable with UV-light	[26]
Silver nanoparticle ink [42]	Sigma Aldrich	Ethylene-Glycol	30%		
Silver nanoparticle ink [43]	Sigma Aldrich	Tripropylene-glycol-mono-methyl-ether	50%		
Agcite [31]	Nanodimension	Undisclosed	Undisclosed	Sintered using infrared-light Proven compatability with ND 1092 ink	
SilverjetP series [2]	Advanced Nano Products	Triethylene-glycol-monoethyl-ether	30-35%	Sinterable with UV-light Proven compatibility with TPGDA	[39]
SilverjetH series [2]	Advanced Nano Products	Tetradecane	50-60%		
NBSIJ-MU0 [41]	Mitsubishi	Ethylene-Glycol	Undisclosed	Chemically sinters on specific substrates	

2.2.3. Sacrificial material

To allow printing of fully three-dimensional structures, a sacrificial structure must be producible to support areas of the printed part that are not in contact with the build-plate. In other 3D-printing processes such as FDM and SLA, these areas, called overhangs, are typically supported either by printed structures with a weak geometry, allowing them to be mechanically broken off, or by a secondary material that can be dissolved in water-based solutions.
Additionally, variations and combinations exist where either *only* the direct interface layers are printed in soluble materials, or non-soluble materials are used that bond poorly to the main structural material.
In Inkjet and Polyjet printing, the ability to print mechanically weak geometries is more limited, and therefore a sacrificial material is chosen that can either be dissolved or has a gel-like structure that can easily be removed mechanically. This material forms a substrate on which the layers of structural material can be deposited. When this support structure is required to be a thin or tall structure, it is possible to print only the interface layers in the weaker sacrificial material, whilst printing the rest of the support structure in a stronger structural material. [7]
In the area of academic research, the subject of Inkjet-printable support material is less thoroughly explored, although mixtures of Tripropylene Glycol Diacrylate (TPGDA) and Triethylene Glycol Methyl Ether (TGME), have been shown to be jettable and result in soft, gel-like material that can be separated from structural material manually. [14]

2.2.4. Material compatibility

When combining conducting and insulating materials in Inkjet-printing, the compatibility of the materials is of great importance. In literature, the aspects that most prominently determine their compatibility are the adhesion of the conductive material to the structural material, and the ability of the structural material to withstand the sintering procedure of the conductive material.

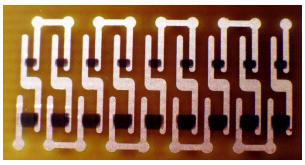
Nanoparticle inks are most commonly either water- or alcohol-based, thus they adhere well to hydrophilic surfaces. As the structural material is polymer-based, it is typically not hydrophilic, and sometimes hydrophobic. This results in a large contact angle, and the beading up of the nanoparticle ink, which prevents the accurate printing of thin traces.
The wettability can be improved through the addition of surfactants to the nanoparticle ink, or plasma treating the substrate layer before depositing the conductive layer, or by choosing a base solvent that inherently has better adhesion to the structural material.[9]
An additional difficulty is the oxygen-inhibition of the curing of photopolymers. During the printing process, the top-most layer is exposed to oxygen-containing air, which can result in improper curing.
For printing of structural material, this can be beneficial as it can improve the bonding of the subsequently printed layers, however for printing electronics this can be detrimental as the uncured polymer can act as a hydrophobic substrate for the nanoparticle ink. [9]

The need for sintering of the nanoparticle suspension also imposes specific requirements on the structural material; In the case of thermal sintering, it must be sufficiently resistant to the high temperatures. In the case of photonic sintering, it is preferred that the structural material does not have a significant absorption peak near the wavelength of the applied light, as to prevent undesired heating of the structural substrate layer.

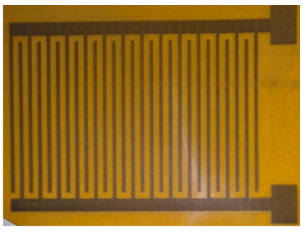
And finally, in the case of chemical sintering, the structural material must be taylored to include the specific required chemicals that induce the sintering of the nanoparticles.

2.2.5. Printing of circuit building-blocks

Several passive electronic components can be constructed from just a conductive and a non-conductive material, allowing them to be printed from the aforementioned materials.
Resistors can be printed as planar traces, where the resistance can be finely adjusted by varying the width and length of the trace. Alternatively, higher resistances can be achieved by using conductive materials with higher resistivities, such as conductive polymers or carbon based inks.
Capacitors and inductors typically require multi-layer circuits, where an insulating material is printed over the conductive traces, allowing traces to cross without making contact. Inductors can be constructed as planar spirals, and capacitors as two flat pads stacked on top of each-other, separated by insulating material, where the insulating material acts as the dielectric. [5] Variations exists however, where single-layer geometries are used to print both capacitors and inductors.
Another building block commonly found in printed circuit boards is the via, which is a structure that acts as a vertical interconnect between circuit layers. A similar structure can be printed using Inkjet-processes, and several geometries have been demonstrated in literature, shown in Figure 2.5. These structures range from simple stacked layers [45] to ramps [11] and helix structures [39].



(a) Series array of resistors, Inkjet printed in conductive polymer on silver electrodes [4]



(b) Planar capacitor Inkjet-printed from a graphene-derived material [44]



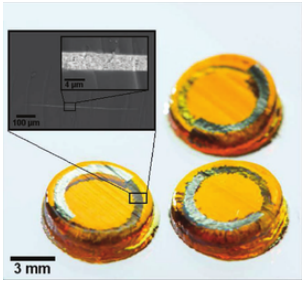
(c) Planar inductors printed from silver nanoparticle ink [27]



(d) 3D-Printed via constructed from stacked layers of silver nanoparticle ink, printed on the FPM Trinity [11]



(e) Diagram of the ramp-style vias, applied in the FPM Trinity system [11]



(f) 3D-printed helix-style vias, printed from silver nanoparticle ink on a Pixdro LD-50 printer [39]

Figure 2.5: Examples of Inkjet printed variants of common electronic components and structures

2.3. Model preparation software

Before an object can be 3D-printed, it needs to be prepared into a format that can be processed by the printer.
Generally, objects are first designed in CAD software, where the shape of the object is described as a sequence of parametric 3D operations. Next, the object is exported as a mesh, where the outer surface of the model is described as a set of triangular polygons. The mesh file is then processed by the 3D printer-preparation software, commonly called a *slicer*, and converted into a printer-specific format containing sufficient information for the printer to construct the object.
As different additive manufacturing technologies utilize completely different methods for constructing objects, slicers are typically platform-specific, although with the recent trends of desktop FDM and SLA 3D printers, it is becoming more common for slicers to support multiple printing platforms.

2.3.1. 3D-printer slicer functionality

Although slicers for different printing technologies can vary greatly in their working and interface, several features can be found in most, if not all, slicers. These include:

- 2D slice generation
- Toolpath generation
- Support generation

2D slice generation

As most 3D printing strategies rely on the stacking of 2D layers, an algorithm must be used to convert the 3D model into 2D slices, from which the term 'slicer' originates.
As the 3D model is typically described as a mesh, this slicing algorithm can be described as a polygon boolean operation, namely an intersection of the model and a horizontal plane. The output of this operation is a 2D polygon that describes a cross-section of the model, and is then sent to the toolpath generator.

Toolpath generation

The 2D polygon resulting from the boolean operation needs to be processed into a format which can be produced by the printer. This step is heavily platform dependent, and can range from rendering the polygon as a monochrome bitmap in the case of SLA 3D printers, to the generation of extruder toolpaths in the case of FDM 3D-printers.
More complex features during this process include the generation of infill patterns for FDM 3D printing, determining the colors of layer contours for full-color Polyjet printing, or even thermal-mechanical modelling in the case of SLM 3D printing. The output of this operation is a set of data or commands that can be directly processed by the printer.

Support generation

The generation of support structures is necessary for 3D printing techniques where there is no supporting medium present, which is the case in Polyjet, FDM, SLA, or where internal stresses would deform unsupported structures, such as in SLM.
These support structures anchor overhanging parts of a printed layer either to the build-platform, or to previously printed layers, thereby allowing the printing of fully 3D shapes. Different strategies exist for generating support structures, and these are often platform dependent. In SLA printing, support structures are generated as meshes before the object is sliced, whereas in FDM the supports are generated directly as extruder toolpaths after the layer has been sliced. Typically, methods are implemented in the generation of these support structures to ease with their removal. This may include weakening the support where it interfaces with the model, or generating the interface layers in a material that may dissolve or doesn't bond to the structural material.

2.3.2. Slicers in inkjet-3D-printing

Due to the proprietary nature of inkjet-3D-printing platforms, there has been limited open-source development of slicing tools specifically tailored for this technology.
Inkjet systems are typically designed to print bitmap images, which makes it feasible to adapt slicing

software originally developed for printing, as both technologies utilize bitmap outputs.
As SLA printing has become increasingly accessible for consumer use, several open-source or free SLA slicers are now available. The bitmap files generated by these slicers can optionally be further processed using custom scripts, to incorporate support structures or other functional modifications. [6]
Alternative approaches reported in literature include generating bitmaps directly using a scripting language such as MATLAB. This method allows for the creation of complex geometries through parametric functions. Another manual method includes designing the bitmap layers individually in image editing software. [39]

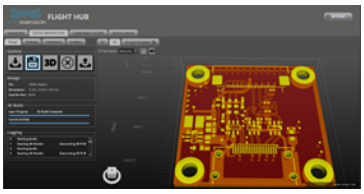
2.3.3. Electronics integration

In additive manufacturing workflows, 3D forms are typically modeled using 3D computer-aided design (CAD) software, while electronic circuits are developed with specialized printed circuit board (PCB) design tools. Modern CAD software has increasingly integrated features that allow importing 3D models of circuit boards into mechanical designs. Furthermore, some advanced CAD programs now include functionalities for creating electronic schematics and PCB layouts directly within the same environment.

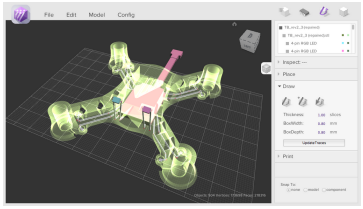
Despite these advancements, current software is predominantly restricted to the design of planar, PCB-based electronics and does not utilize the capabilities and design freedom provided by 3D-printed electronics.
One straightforward but labor-intensive approach for designing 3D-printed electronics, involves designing electronic elements in the same manner as structural components—by using 3D forms. However, as circuit complexity increases, this method becomes impractical and cumbersome [50].

To address these challenges, several commercial software solutions have been developed, such as Nanodimension's Flight Hub [10] and Project Wire by Voxel8 [54]. These platforms provide dedicated tools for embedding electronic components within 3D structures, streamlining the design and slicing processes, and aid in the routing of conductive traces between components.

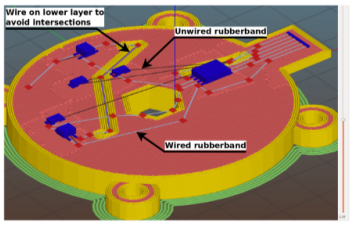
An alternative approach has been proposed by Wasserfall et al., and involves utilizing existing open-source slicer software, augmented with custom plugins for electronic design. The layer-by-layer processing nature of slicers lends itself well to adopting a PCB design-like interface, where components can be arranged in layers, traces can be routed, and vias connecting different layers can be introduced [50] [51].



(a) Nanodimension Flight Hub, a software suite for designing and slicing 3D-printed electronics [10]



(b) Project Wire, a software tool for integrating electronic circuits into mesh-based models [54]



(c) Slic3r plugin for importing models of electronic components and generating circuit traces [1]

Figure 2.6: A selection of slicer programs with the functionality to embed electronics into the structural material

3

Printing setup

3.1. Pixdro LP50

The Pixdro LP50 (also known as the SUSS LP50) is an inkjet development platform designed for research and development in inkjet printing processes, as well as the evaluation of inkjet materials and printheads. The system features an A4-size aluminum buildplate (227 x 327 mm), which can be heated up to $90°C$. This build plate also serves as a vacuum table, enabling secure fixation of large substrates through suction.

The system is equipped with five independent axes of motion, those being the X, Y, and Z linear stages, along with rotational axes for the printhead and the printbed. This configuration enables high-precision positioning with micrometer-level resolution in both the horizontal and vertical directions.

For real-time droplet analysis, the system utilizes a camera with a stroboscopic light. Additionally, a microscope camera is mounted on the printhead, allowing for inspection and analysis of the deposited patterns.

The system includes an automatic wiping station to clean the printhead, as well as a capping station that serves two functions: protecting the printhead from UV exposure and applying negative pressure for printhead unclogging when necessary.

A stationary UV-light bar (Phoseon FireEdge FE300) is mounted directly above the printing platform. This high-power lamp allows for curing UV-sensitive photopolymers and for sintering nanoparticle materials.

3.2. Printhead

The system features a modular design, enabling the integration of various printhead types. The printhead mount features a kinematic coupling, allowing for quick manual switching, which is particularly advantageous for multimaterial printing.

The printhead-specific electronics, including the wave generator for the piezoelectric elements, are housed in the head personality box (HPB). Two HPBs can be accommodated in the printer simultaneously, allowing for concurrent multimaterial printing, provided this is supported by the printhead.

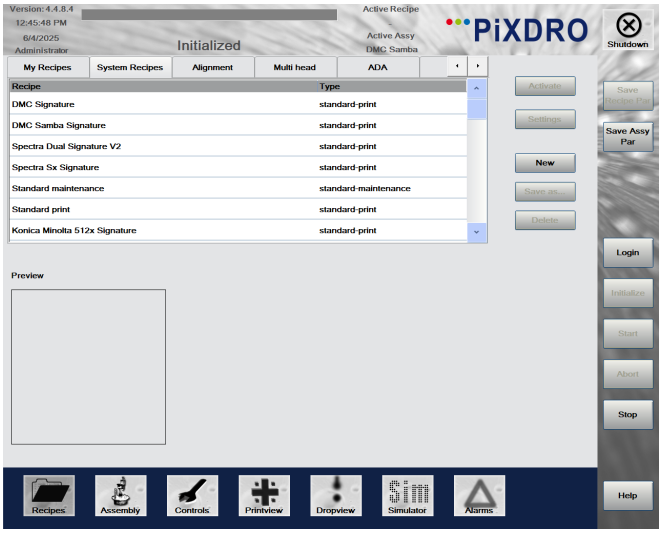
A pressure control system capable of generating both positive and negative pressures is implemented. This system is capable of compensating for the hydrostatic pressure due to the liquid column in the printhead, and of purging the nozzles by forcing ink through the printhead nozzles with positive pressure.



Figure 3.1: Pixdro LP50 Inkjet development platform



(a) Pixdro Printhead Assembly, with a Dimatix print cartridge installed. Visible in the background is the accompanying Head Personality Box.



(b) Screenshot of the Pixdro HMI software

3.3. Pixdro HMI

The Pixdro Human Machine Interface (HMI) is the platform's accompanying software, which allows for direct control of many of the system's functions, as well as the generation of toolpaths for printing bitmaps and the analysis of ejected droplets.

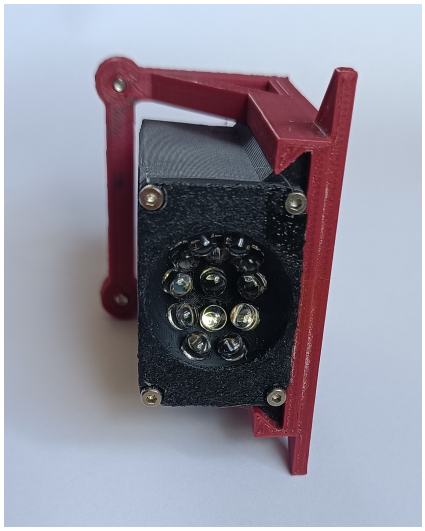
Key parameters of the jetting process, such as the analog waveform, frequency, negative pressure, and temperature, can be tuned in the HMI. The resulting droplets can then be analyzed using the integrated stroboscopic camera. Additionally, droplet velocity can be measured automatically through machine vision in order to calibrate the droplet Time of Flight (TOF) for bidirectional printing.

The HMI also supports scripting in C#, which allows for programmatic control of machine parameters, motion systems, and the execution of print jobs.

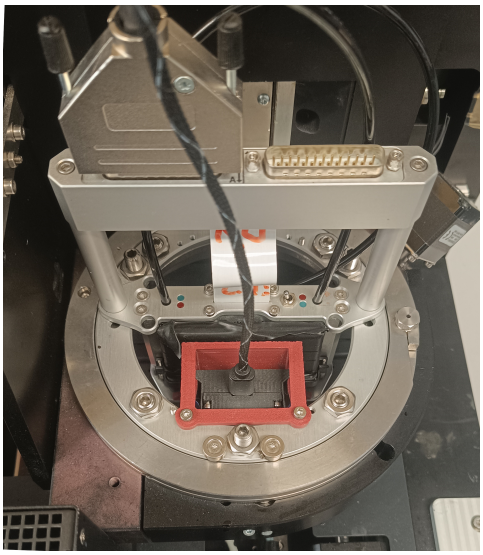
3.4. Modifications for 3D-printing

As the Pixdro LP50 is an inkjet development platform, it contains pre-made software routines for the printing of 2D patterns. To enable its use for 3D printing applications, custom scripts are required to execute successive print jobs, raise the printhead between layers, and cure each printed layer accordingly.
In this work, a script developed by Davenne et al.[6] is used in modified form, which has the capability to print a set number of bitmaps, UV-cure the printed layers for a set duration, and raise the printhead according to the set layer height. Additionally, during curing, the printhead is positioned at the so-called *service position* at the lowermost position to minimize stray reflections of UV light on the printhead.

To enable the curing of deposited material during the process of printing a layer, an additional, less powerful UV-light module was mounted directly on the printhead. This custom module contains 13 14mW UV LEDs in a hemispherical configuration focused at a single point, which is offset 35mm from the printhead nozzle array. Direct integration of the UV module with the existing software proved challenging. As a solution, the module was equipped with a micro-controller and a MEMS gyroscope module. This configuration allows the UV light to be turned on and off through a specific, pre-programmed printhead maneuver, namely, a quick clockwise rotation followed by a counterclockwise rotation.



(a) View of the bottom of the UV-module, showing the 13 UV-LEDs in a hemispherical configuration.



(b) UV-module as mounted in the printhead, located directly next to the print-cartridge. Power is provided by a USB cable.

4

Model preparation software

To enable inkjet-3D-printing of structural electronics, several pre-processing steps are required to convert a digital design into a format compatible with the inkjet printer.
As discussed in section 2.3, there is currently a lack of open-source slicers capable of preparing models specifically for inkjet-3D-printing. Moreover, to support the fabrication of structural electronics, it is desirable to have a software tool that allows the integration of electronic circuits into 3D models, and ideally provides a 3D preview of the generated model as a visual aid.
This chapter addresses this gap in the current state of the art by presenting the development of a dedicated slicer for Inkjet 3D printing. The tool integrates several features to support the design and manufacturing of structural electronics.
section 4.1 outlines the requirements that have been set for this slicer program. section 4.2 describes how these features are implemented and how the underlying algorithms function.

4.1. Slicer requirements

The development of the slicer began with the formulation of key functional requirements. These are as follows:

1. Ability to slice 3D models to a format that can be inkjet-printed.
2. Visualization of the sliced model through a rendered preview.
3. Generation of support structures for overhanging regions.
4. Tools for the design and placement of electronic circuits.
5. Integration of both planar and non-planar circuits into the structural geometry.
6. Generation of interconnects for multi-layer circuit designs.
7. Embedding of electronic components within the sliced model.

The first three requirements refer to features that are found in most conventional 3D slicers, and are deemed as essential for any basic slicing program: model slicing, preview rendering, and support material generation.
Requirement 4 reflects the need to integrate circuit design capabilities directly into the slicer. This allows users to design circuits in context, referencing the 3D geometry during layout, unlike workflows that rely on external circuit design tools.
The final three requirements are specific to the embedding of functional electronics within printed structures. They aim to enable features such as multi-layer interconnects and the integration of electronic components into the structural material, thereby supporting the fabrication of fully functional structural electronics.

4.2. Slicer implementation

Based on the defined requirements, a slicer tool was developed using the programming language Python. Several libraries were utilized to enhance the efficiency of mathematical operations, allow for efficient rendering using OpenGL, and interfacing with GUI elements. A simplified diagram illustrating the main program loop for the slicing process can be found in Figure 4.1. Furthermore, the implementation of the features specified in the requirements is explained in the following section.

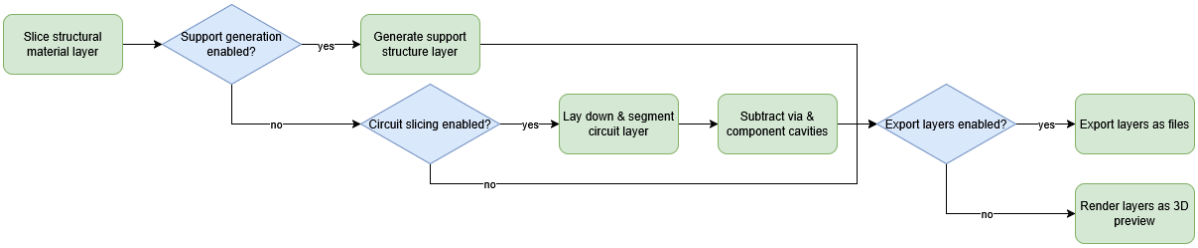


Figure 4.1: Structure of the main slicing function, which is performed on each layer

4.2.1. Structural material slicing

The industry standard file format for 3D-models for additive manufacturing is the STL format. In this format, which was created specifically for the purpose of additive manufacturing, models are represented as a collection of triangular polygons, making up the outer surface of the model. While more advanced formats such as STP (STEP) and AMF (Additive Manufacturing File Format) are available, their increased complexity limits their adoption, and they are not widely supported by slicers.
The STL format does have certain downsides, as it allows the creation of non-manifold models: models where there is no clear distinction between the inside and outside of the models. Such issues are more common in models created using mesh-based modeling tools and occur less frequently in STL files exported from parametric CAD software.
The Pixdro LP50 printer used in this project requires image-based input data. It supports formats such as PNG, BMP, and GIF, which can be directly imported via the Pixdro HMI and printed without detail loss. Although formats like JPEG are also supported, their lossy compression may degrade print quality.
As discussed in section 3.4, a custom script is already present in the Pixdro HMI to enable printing of a sequence of bitmaps (bitmap stack). Thus, in order to utilize this printer for 3D printing purposes, the slicer has to slice the 3D STL files into an array of 2D bitmaps. To achieve this, an algorithm is developed that performs this in three steps:

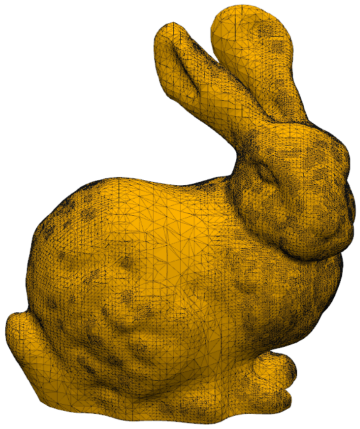
1. **Intersection Calculation:** For each triangular polygon in the STL file, the intersection with the slicing plane is computed. Polygons intersecting the plane produce line segments, while non-intersecting polygons are discarded.
2. **Layer contour generation:** Laid together, these line elements form a contour that represents a horizontal slice of the model, which is called the layer polygon. An example of such a layer polygon, and the model from which it results, can be seen in Figure B.4 In the case that a model has internal voids or is split into multiple elements at the slice, several closed loops may be the result.
3. **Layer rendering:** The layer polygons are rasterized by a scan-line algorithm, which calculates the intersection between a scan-line and the line elements, and fills the section between the intersection points in a 2D array. Performing this for all scan-lines results in a 2D bitmap that represents the layer polygon.

This algorithm is performed for every layer, which finally results in a voxelized version of the STL model. A pseudocode summary of the algorithm is as follows:

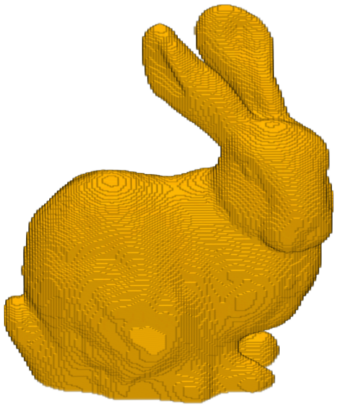
Algorithm 1 STL slicing algorithm

```
for each slicing layer do
    for each STL polygon do
        if STL Polygon Intersects layer then
            Calculate intersection points
        end if
    end for
    Construct layer polygon
    Rasterize layer polygon
end for
```

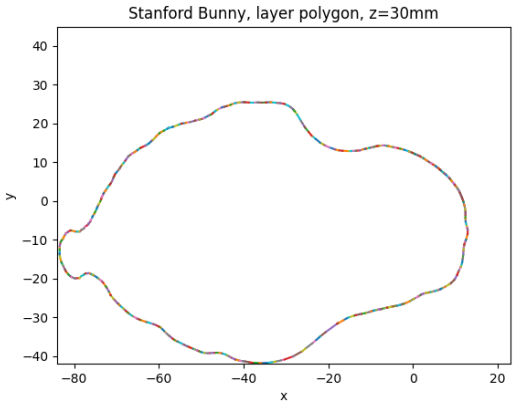
This algorithm is implemented in python, where many of the computationally-intensive operations are performed in Numpy, greatly improving the performance of the algorithm.



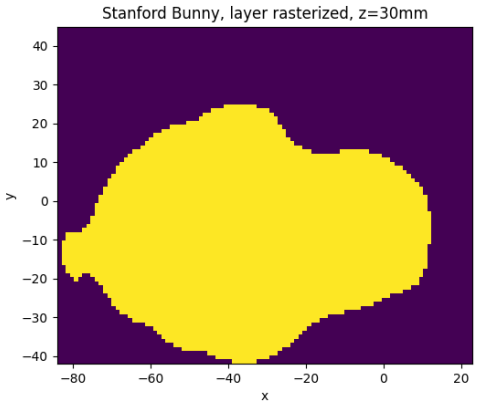
(a) STL model, highlighting the polygons making up the outer surface



(b) Model after slicing, displayed as a stack of rasterized images



(c) 2D slice of the Model, at z=30mm, displayed as a polygon



(d) 2D slice of the Model, at z=30mm, rasterized into a bitmap

Figure 4.2: Example of the slicing algorithm as applied on the Stanford Bunny model.

4.2.2. GUI

To aid in visualizing the sliced models, a GUI and 3D rendering system were developed to display the STL model and the sliced model data. The implementation utilizes the Pyglet library, which provides Python with access to OpenGL rendering methods, allowing efficient rendering of 3D models.
Given that most 3D rendering methods are based on rendering polygonized models, STL models are simple to import and can be rendered very efficiently. In the slicer, the STL model is almost directly streamed to the vertex buffer. Shaders are used to highlight model features, by calculating the bright-

ness of a polygon based on its surface normal.
In contrast, the sliced model data is volumetric and does not conform to conventional polygon-based rendering approaches. In the developed slicer, the rendering of this is implemented by rendering every sliced bitmap into a 2D texture. These textures are then mapped onto a stack of square polygons, where each polygon represents a discrete, sliced layer, giving the illusion of 3D. This technique, which is a variation of the shear-warping algorithm, gives satisfactory results at higher viewing angles and allows for intuitive navigation through individual layers. However, it introduces visual artifacts when observed from lower angles. To partially mitigate this, each layer plane is rendered ten times, each time slightly vertically offset, to give an illusion of depth to individual layers.
A virtual build-plate is rendered to provide a spatial reference, and other GUI elements, such as buttons, are accompanied by icons that visually represent their functions.

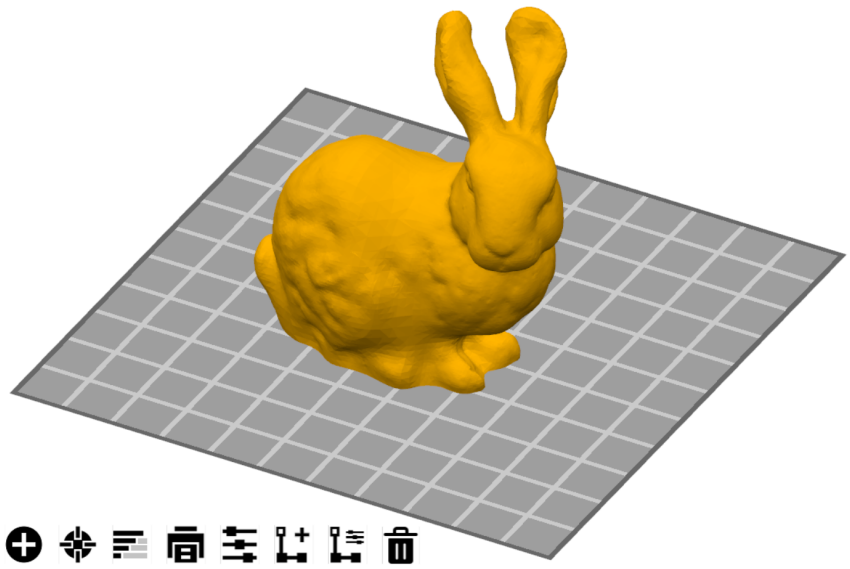
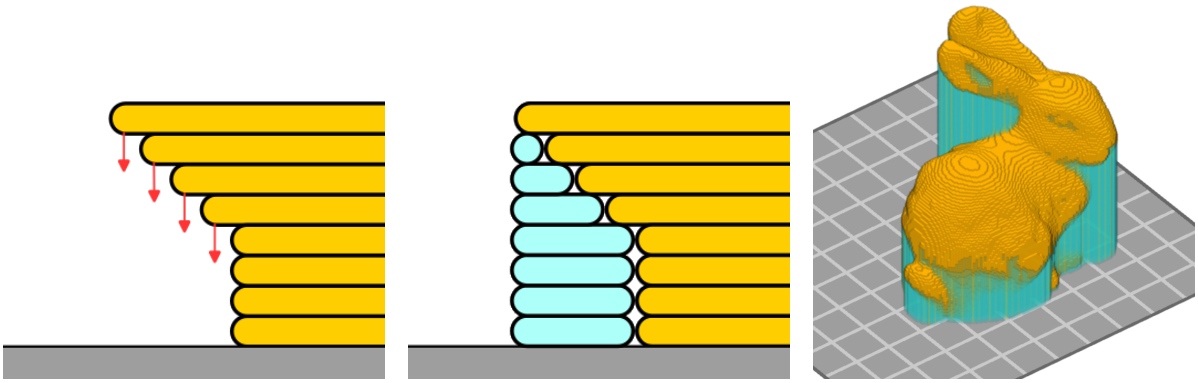


Figure 4.3: Screenshot of the developed slicer, showing the buildplate, GUI buttons, and a loaded STL model

4.2.3. Support generation

As the process of inkjet printing relies on droplets being ejected downwards, it is not possible to print any overhanging geometries in the manner that FDM and SLA are able to. In order to still produce such geometries, a removable support material can be utilized, which enables the printing of fully 3D geometries.
Similar to FDM and SLA slicers, the developed inkjet slicer can automatically detect overhanging areas and generate a structure of support material. Contrary to FDM and SLA slicers, however, this process is not performed on the STL model but rather on the rasterized model, on a pixel-by-pixel basis. The slicer rasterizes the STL models from top to bottom and stores a mask of pixels that have been occupied by structural material. If a pixel is detected where no structural material is present, but the mask indicates that structural material is present above the current pixel, a pixel of structural material is generated.
As this algorithm is performed for every layer, a structure of support material is generated that acts as a scaffold, and ensures that every pixel is either supported by structural material or support material.

Typically, inkjet-printable support materials have poor mechanical properties and are prone to sagging and deformation. To improve the structural rigidity, it is common to intermix a pattern of structural material into the support structures, such that the mechanical properties of the support structure are a mix of those of the support material and the structural material.
In the slicer, this is a feature that can be enabled by the user, where a grid of structural pillars with a set density is generated within the support structure.



(a) Layer-by-layer view of an overhanging structure, the arrows indicate material that would fall down during printing.

(b) Layer-by-layer view of an overhanging structure, showing how a support structure would be generated.

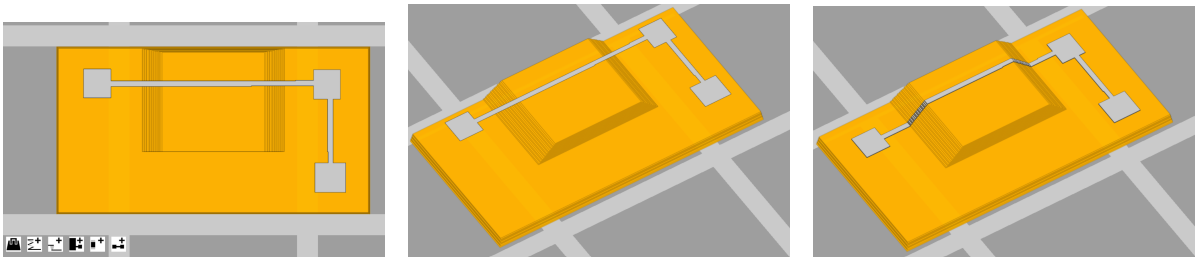
(c) Slicer view of the automatically generated supports on a model with overhanging features.

Figure 4.4: Illustration of the support generation algorithm in the developed slicer

4.2.4. Circuit designing

To aid in the design of 3D circuit elements, the slicer contains tools to lay down conductor traces and pads on structural material. These conductor elements are placed on so called *circuit layers*. Circuit layers are horizontal layers that can be created on any sliced layer within the model, and form a canvas for designing circuits. Following principles similar to those found in traditional PCB design software, traces can be created by selecting a start point and an end point. Pads are created by selecting two diagonally opposite corners, forming a rectangle.

In the literature, it has been reported that a layer of printed silver is 5-10 times thinner than a layer of printed polymer. [39] This, in combination with the fact that the silver won't be used to form 3D structures, has led to the decision to assume that the circuit layers have a thickness of 0 in the slicer program. It is treated purely as a 2D structure, which may be positioned on top or in-between the voxels of structural material.
When slicing the model with created circuit layers, the user can choose the circuit rendering method. Circuits can be displayed as zero-thickness layers at the height where they are designed. Alternatively, the user can enable the slicer to account for a 3D substrate when rendering the circuit layers: Circuit elements that are positioned directly on structural elements are rendered flat at that height, but circuit elements that are positioned floating above a structural layer or are placed on a geometry that is not flat are laid down to conform to the underlying geometry. In this rendering method, the circuit layers are rendered as if they have the same thickness as structural layers, but they are still assumed to be zero-thickness layers. A screenshot of the circuit designer mode, along with both rendering methods, is provided in Figure 4.5.



(a) Screenshot of the circuit design mode in the developed slicer, with a simple example circuit containing pads and traces.

(b) 3D view of the designed circuit superimposed on a non-planar structure. The circuit is rendered as a flat plane positioned on the sliced model.

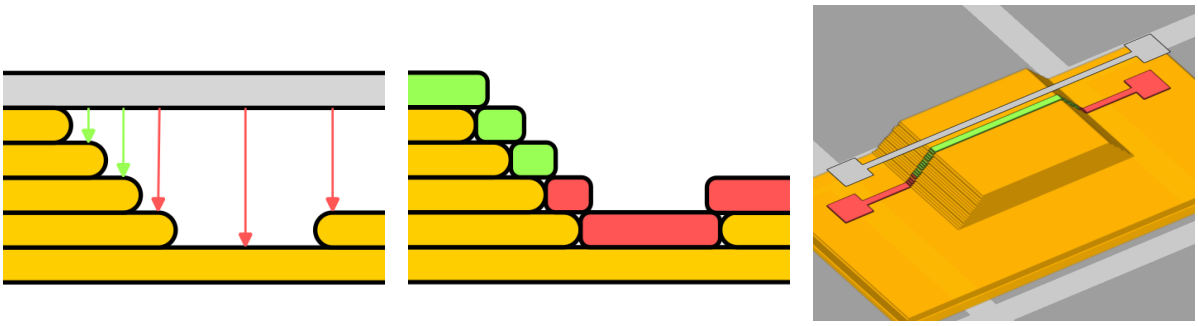
(c) 3D view of the designed circuit after it has been sliced. The circuit is laid down on the non-flat surface of the sliced model.

Figure 4.5: Procedure for designing and slicing electronic circuits in the developed slicer

4.2.5. Circuit vertical segmenting

A key advantage of inkjet printing is that the printhead is not in touch with the substrate, and can in fact be positioned several millimeters above the substrate. This property is utilized to enable the printing of 2.5D circuits, by printing a 2D circuit design on a non-flat substrate, as shown in Figure 4.5.

There is, however, a limit to this distance between the printhead and the substrate, after which the accuracy of the droplet deposition begins to decrease. Therefore, one must ensure that when printing on a non-flat substrate, the height of vertical features of the substrate must be lower than the allowable jetting height of the printhead.
To address this constraint, the slicing software includes an option to automatically detect if parts of circuit layers fall below the allowable jetting height. In the case that such regions are identified, they are split off from the circuit layer and are scheduled to be printed at an earlier stage, at a lower height. This segmentation process is applied concurrently across all circuit layers. It may also merge segmented portions from different circuit layers into a single printable pattern if this is deemed favorable by the slicing algorithm. This procedure, referred to as *vertical segmenting*, enables the printing of circuits with theoretically indefinite height, limited only by the range of motion of the system's z-stage.
Figure 4.6 illustrates this concept; A circuit layer is laid down on a substrate with a feature that exceeds the allowable jetting height. Therefore, this circuit layer is split into two sections, visualized as green and red, where the red section is printed at an intermediate height, and the green section is printed at the final height of the model.



(a) Layer-by-layer view indicating how a circuit (gray) is laid down on the substrate. At certain areas the jetting height is too large.

(b) Layer-by-layer view indicating how the circuit conforms to the substrate. The red circuit segments need to be printed at an intermediate step.

(c) Slicer view of a circuit (gray), which has been split into two segments (red & green), due to spanning a vertical distance exceeding the jetting height.

Figure 4.6: Algorithm for splitting circuits into segments, based on the maximum allowable jetting height. Note that although the circuit trace is illustrated with the same thickness as a structural layer, it is deemed as a zero-thickness layer in the slicer.

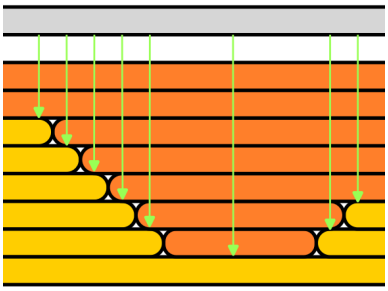
4.2.6. Non-planar embedded circuits

The aforementioned process of laying down and slicing of circuits allows for the printing of *non-planar* electronic circuits on top surfaces, and *planar* circuits embedded in structural material, but not yet the printing of *non-planar* embedded circuits. For this purpose, another slicing method can be enabled, namely *sandwich*-slicing. In this method, a model can be imported in multiple segments, where the first model segment serves as the primary structure and the other segments are secondary structures that are printed on top of the main structure. The primary structure now serves as the substrate for the circuit layer, and the secondary structures are printed over the primary structure and the circuit.
As the secondary structures are printed *over* the primary structure, the printhead should be positioned at a height sufficient to ensure the printhead does not collide with the primary structure. This has two consequences:

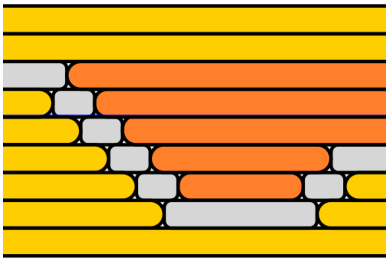
- Layers of the secondary structures that are positioned below the maximum height of the primary structure can be printed without increasing the printhead-height in between layers.
- A validation step is necessary to ensure that these layers do not extend below the maximum allowable jetting height.

For these reasons, layers of the secondary structures are exported in separate batches; sections of the secondary structure that lie below the maximum height of the primary structure are exported in a batch

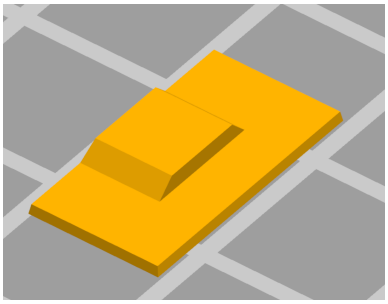
which is to be printed from a fixed printhead-height. The other sections of the secondary structure, those that lie above the height of the primary structure, are to be printed with the printhead moving up by a layer height for each layer.
To ensure the maximum jetting height is not exceeded, an algorithm checks if the lowest part of the secondary structures differs from the highest parts of the primary structure by more than the maximum jetting height. If this is the case, the secondary structure and the circuit layer that lies in between are segmented vertically, according to the algorithm explained in subsection 4.2.5.



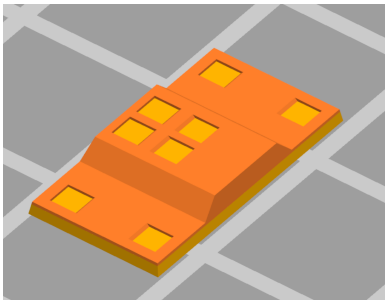
(a) Layer-by-layer view, showing how a circuit layer (gray) is laid on top of the primary structure (yellow), but under the secondary structure (orange).



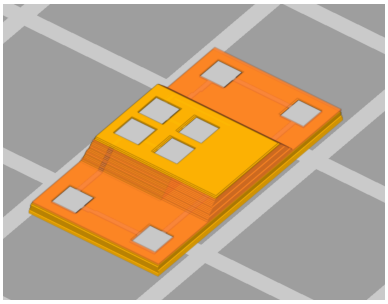
(b) Layer-by-layer view, indicating layers that are printed while increasing the printhead-height (yellow), and layers that are printed with a fixed printhead-height (orange).



(c) Slicer view of the primary structure (yellow)



(d) Slicer view of the primary structure (yellow) and the secondary structure on top (orange)



(e) Sliced sandwich circuit, yellow layers are printed while increasing the printhead-height, orange layers are printed with a fixed printhead-height.

Figure 4.7: Example of the sandwich slicing method, in a layer-by-layer view (a, b), and in the slicer (c, d,e)

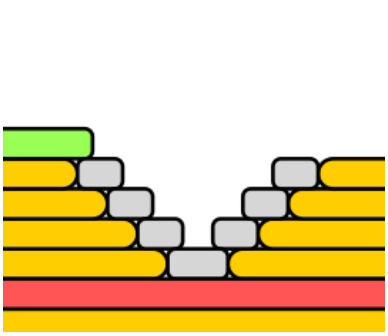
4.2.7. Via generation

It may occur that several circuit layers are designed on a model, but at differing heights. In this case, a user could connect these circuits by designing diagonal ramps into the 3D model, onto which traces can be laid down, thereby spanning a vertical distance.
It may, however, not always be convenient to design these features in the original CAD model, as the user would need to plan in advance how the circuit would be placed on the model. For this reason, a feature is present to generate interconnect structures in the circuit design mode.

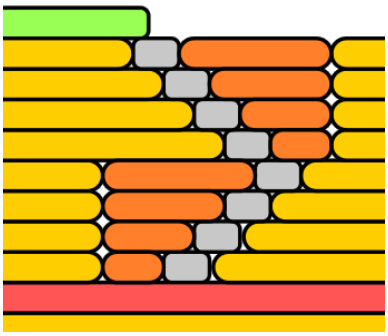
The most conventional strategy for printing such features would be to stack layers of printed silver vertically until the desired height is reached, similarly to how layers of structural material are stacked to form 3D shapes.
However, as the layer thickness of the printed silver is on the order of several microns, and each silver layer needs to dry and be sintered, this would take hundreds or thousands of sintering cycles to accomplish, which would increase the print-duration to an excessively long time.

For this reason, a different strategy is chosen, for which the term *dimple-via* is chosen. Similar to vias in conventional PCB design, dimple vias consist of a conical hole in the structural layer, which is coated with conductive material. Only a single layer of conductive material needs to be deposited to accomplish this, while it spans a vertical height of tens or hundreds of layers of structural material.
In the slicer, dimple vias can be created in a circuit layer, and connect to a different circuit layer either above or below the initial circuit layer, thereby forming a vertical interconnect.
During the slicing process, for each layer a check is performed if vias are present at the current height. When this is the case, the hole required for the dimple via is subtracted from the structural layer. Since the hole has a conical shape, the size of the hole that needs to be subtracted increases with height, such that the walls are sloped.
As silver needs to be printed in these internal walls, there is a limit to how steep the walls can be, which in turn limits the height a dimple via can span.

For spanning more significant distances, a second interconnect structure is proposed, for which the name *stairwell-via* is chosen. In this method, a triangular prism-like cavity is created in the layers of structural material, creating a ramp. On this ramp, a trace of silver is printed, and the hole is filled in with resin. On top of this structure, the structure is constructed again, but in the opposite direction now, such that the circuit trace ends up vertically above the starting point. Depending on the height that needs to be spanned, several sets of ramps can be stacked, which results in a structure that resembles a stairwell. A circuit trace printed on a ramp can be printed in a single layer, but can span many layers of structural material, thereby allowing the bridging of significant vertical distances, with a small number of silver sinter cycles.
Similarly to dimple-vias, stairwell-vias can be placed in circuit layers in the slicer, after which the via structure is automatically integrated into the layers of structural material.



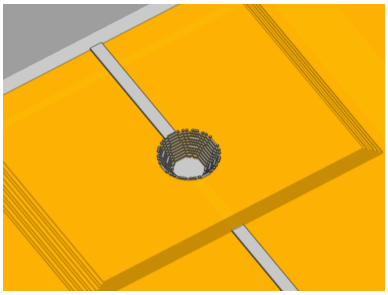
(a) Two circuit layers (red & green) are connected vertically through a dimple via, a hole in the structural layers, covered in silver (gray).



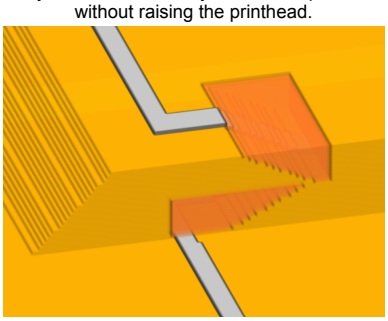
(b) Two circuit layers (red & green) are connected vertically through a stairwell via, two consecutive ramps of silver (gray) embedded in the structural layers. Orange layers indicate filler layers that are printed without raising the printhead.



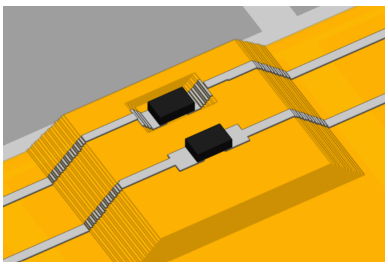
(c) A component (black) is recessed into a cavity in the structural layers.



(d) Dimple-via connecting two circuit layers separated by a small vertical distance.



(e) Stairwell-via connecting two circuit layers separated by a larger vertical distance.



(f) Two 0805 SMD resistors, one laid onto a circuit layer, one recessed into a circuit layer.

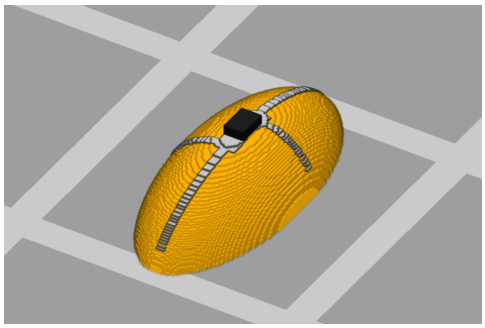
Figure 4.8: Layer-by-layer views of the dimple-via, stairwell-via, and embedded components, and their representation in the developed slicer program.

4.2.8. Component importing and slicing

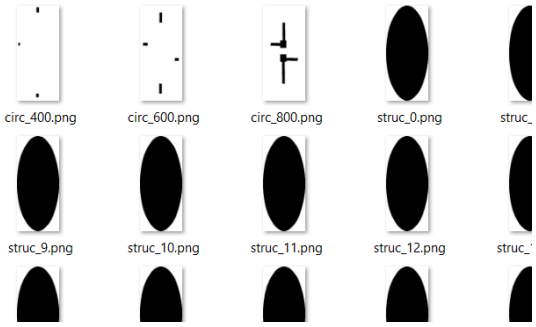
The integration of electronic components is essential for the realization of a functional circuit. These components may range from basic elements such as resistors and capacitors to more complex devices like integrated circuits.
Within the circuit design mode of the slicer, electronic components can be placed onto the circuit. After placing, the component is indicated by the pads onto which the component can be placed. During slicing, a 3D representation of each component is automatically generated to aid in design verification. When a circuit layer is embedded between structural layers, cavities are automatically generated in the structural layers to ensure that there is no interference between the volume of the component and the structure. Through this method, components can be embedded inside the 3D model.
Furthermore, it is possible to configure components to be recessed into the circuit layer. In such cases, an additional cavity is generated beneath the circuit layer to accommodate the component.
The shape of components, their electrical pads, and the generated cavity, are defined as level-set functions in a configuration file, and allow for any arbitrary 3D shape.

4.2.9. Layer rendering & exporting

As explained in subsection 4.2.2, a 3D layer-preview is generated upon slicing, by rendering the layers to a stack of square polygons. Of these layers, the order in which they are printed is retained, allowing the user to scroll through the printing process in time.
To limit the memory usage of the program and to reduce loading times, this rendering is performed at a resolution lower than the final resolution. When the user desires to export a model, the layers are rendered at the final resolution and directly exported to PNG files after generation, and no 3D preview is generated. The exported PNG files are monochrome, where black pixels indicate deposited material, and can describe both circuit layers and structural layers. In Figure 4.9, and example is given of exported layer files. In Appendix B, an explanation is given of the naming convention of these exported files.



(a) Example sliced model: a circuit with a component on an ellipsoid structure



(b) Resulting exported files: The circuit height exceeded the jetting height, and has therefore been split into 3 segments.

Figure 4.9: Comparison between the generated 3D preview and exported layer files

5

Polymer inkjet printing

In this chapter, inkjet-3D-printing of a structural material is investigated. In section 5.1, the required material properties are discussed and a suitable ink is selected. In section 5.3, the tuning process for jetting this ink is discussed. section 5.4 describes how other parameters and aspects relevant to the printing process are tuned. Finally, in section 5.5 the results of the printing process are analyzed.

5.1. Ink selection

As discussed in subsection 2.2.1, a range of different UV-curable inkjet inks has been demonstrated in both the scientific literature and commercial applications. However, the majority of these inks are proprietary in nature, which limits their usability for research purposes. The lack of documentation on exact ink formulations makes it difficult to predict how the ink will handle being outside its normal operating conditions, such as during photonic sintering. Furthermore, commercially available inks may be discontinued at any time, which reduces their reliability for long-term research.
For these reasons, the decision was made to use a TPGDA-based photoresin, which has been demonstrated in several prior studies. [39] [14] This photoresin is comprised of the monomer TPGDA and a photoinitiator and photoaccelerator, which can be mixed with basic laboratory equipment.
Furthermore, this material has been demonstrated to serve as a suitable substrate for AGNP ink deposition, and can withstand the temperatures and UV irradiation that occur during UV sintering.

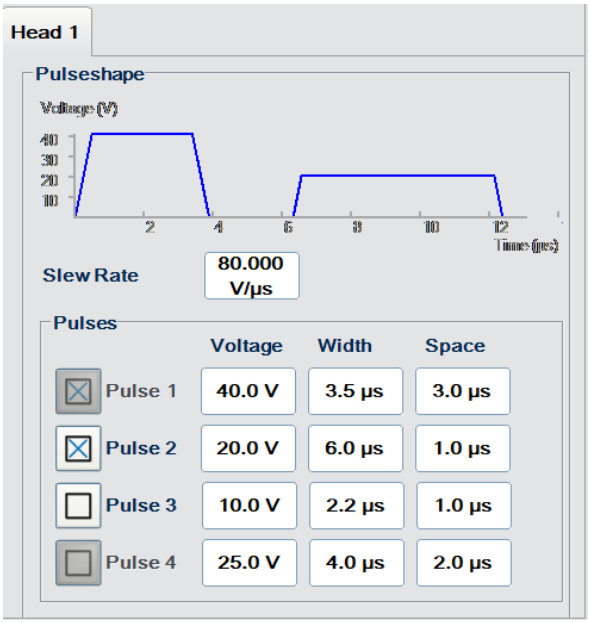
5.2. Ink preparation

The photopolymer resin was prepared by mixing Tripropylene glycol diacrylate (TPGDA) with 3% by mass of 2,4-diethylthioxanthone (DETX) and 3% by mass of 1,2-Dibromoethane (EDB). This mixture was stirred magnetically until fully dissolved, and stored in an amber vial at $5°C$ to inhibit curing.
Photoinitiator amounts of 1%, 2%, and 3% were tested, and no noticeable difference was observed during printing or curing.

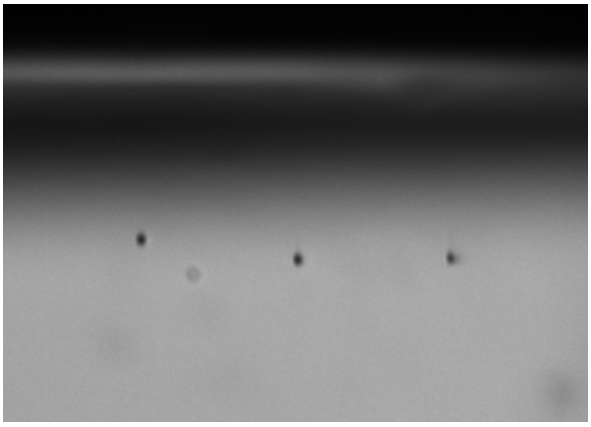
5.3. Jetting parameters

The photoresin was printed using Dimatix Samba material cartridges. These low-cost cartridges are compatible with a large variety of inkjet inks, ranging from particle-loaded aqueous solutions to UV-curable inks, and can be easily replaced in case of persistent nozzle clogging. However, limitations include a relatively small number of nozzles (12), and low volume per droplet (2.4 pL), resulting in the cartridge's native DPI being too low for single-pass printing. Moreover, the cartridges support only low-viscosity inks (ideally 4-8 cps) [13], restricting usable formulations primarily to diluted acrylates. [28]
For generating the pressure wave that results in an ejected droplet, the Samba cartridge utilizes piezoelectric actuators. The exact drive signal used for operating these, called the waveform, is an analog signal that consists of a series of pulses of variable amplitudes and durations. The exact waveform required for clean and consistent jetting depends on the ink used, and can therefore be adjusted manually in the Pixdro HMI.

The waveform parameters were tuned manually until satisfactory results were achieved and are stated in Figure 5.1a.
Furthermore, the Dimatix Samba offers temperature regulation of the ink, which allows the user to fine-tune the viscosity of the ink. In this tuning, a balance, must be found between a low temperature, which results in a high viscosity and less consistent jetting, and a higher temperature, which results in a lower viscosity and less stable droplets. A temperature of $27°C$ was found to yield stable droplets while also allowing consistent jetting for all nozzles.



(a) Waveform used for jetting the photopolymer resin



(b) Resultant droplets, as visible in the Pixdro HMI dropview analysis

Figure 5.1: Jetting parameters used for printing Metallon JS-A211 with the Dimatix cartridge

5.4. Print parameters

5.4.1. DPI, Step Size & Quality Factor

For printing 2D bitmaps with the Pixdro LP50, the image data needs to be converted to a series of toolpaths and jetting commands that can be executed by the printer. This task is performed by a subroutine in the Pixdro HMI, which is called the *motion generator*, that takes in a bitmap and set of parameters, and sends the generated toolpath directly to the printer. Several parameters can be adjusted in this function, with the main parameters that influence the print-data generation being:

- Dots per Inch (DPI)
- Quality Factor (QF)
- Step Size (SS)

These parameters are described in the following sections.

Dots per Inch

The dots per inch describe the number of droplets that are deposited to cover a linear distance of 1 inch. As the droplet volume is essentially fixed by the type of printhead, the DPI directly corresponds to the amount of volume deposited per area.
A very low DPI results in individual, unconnected droplets on the substrate. Raising this value until the deposited droplets barely connect gives the minimum printable layer height. Raising the DPI further increases the layer height but can result in bulging or bleeding of the printed pattern, which negatively impacts the print quality.

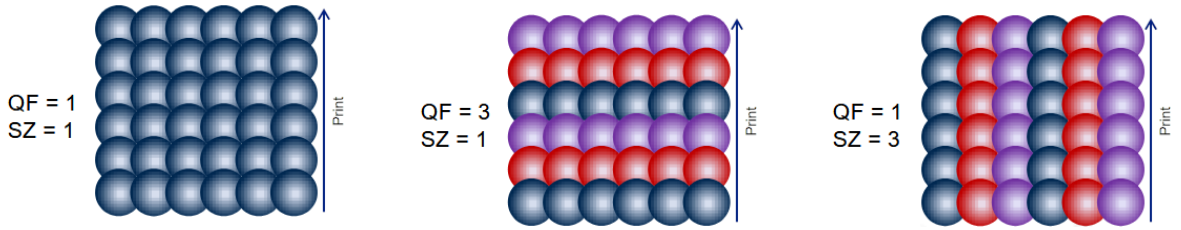
The DPI can be varied independently in both planar axes of the printer. In the scan direction, it can be varied straightforwardly by either increasing the jetting frequency or reducing the travel speed of the printhead. For increasing the DPI in the axis perpendicular to the scan direction, there are two different methods: The printhead can be rotated in the vertical axis such that the array of nozzles is no longer perpendicular to the scan direction, allowing any arbitrary DPI value to be chosen that is smaller than the native DPI. Alternatively, the printhead can make multiple passes over the same area, each time with a small offset, allowing any multiple of the native DPI to be chosen.

Quality Factor

During printing, it may occur that a nozzle becomes defective or clogged and thus cannot jet. In this case, lines of missing material will be visible in the axis of the scanning direction.
This effect can be (partially) mitigated by increasing the quality factor parameter: This parameter determines how many passes are used to print a single line. With a quality factor of 1, each line is printed in a single pass, and thus by a single nozzle. With a quality factor of 2, a single line is printed in 2 passes, by 2 nozzles. As each nozzle then prints half of the droplets in the line, the effect of a defective nozzle is less noticeable. The quality factor can be increased up to the total number of nozzles present, at which point the effect of a defective nozzle can only be detected as a decrease in the total amount of deposited material. A disadvantage of this method is that the time required for printing a pattern also scales with the quality factor: A pattern takes 3 times as long to print with a quality factor of 3 compared to a quality factor of 1.

Step Size

Similarly to the quality factor, the step size is a parameter that can be used to hide defective nozzles; however, only when printing at a multiple of the native DPI. Normally, the multiple passes of a single nozzle are positioned next to each other, which means that the printhead makes a 'step', the size of which is equal to the spacing between the passes. With a higher step size, the step that the printhead makes is equal to the spacing between the passes multiplied by an integer value. This results in adjacent passes being printed not by a single nozzle, but by different nozzles. Therefore, increasing the step size reduces the width of missing lines due to nozzle clogging, which reduces the visibility of the defect. At the maximum step size, a defective nozzle results in missing lines with a width equal to that of a single droplet, which is on the order of $50\mu m$.



(a) Pattern printed with a step size and quality factor of 1. Vertical lines are printed by a single nozzle, and horizontally adjacent lines are printed by the same nozzle.

(b) Pattern printed with a step size of 1 and quality factor of 3. Vertical lines are printed by three nozzles, and horizontally adjacent lines are printed by the same three nozzles.

(c) Pattern printed with a step size of 3 and quality factor of 1. Vertical lines are printed by one nozzle, but horizontally adjacent lines are printed by differing nozzles.

Figure 5.2: Illustration of the effect of the quality factor and step size on the droplet deposition

Chosen Parameters

As it was found that even without defective nozzles there were slight differences in the amount of deposited material by different nozzles, the maximum allowable step size was chosen (the number of nozzles, 12). This greatly improves the print quality with no negative effects on the print-duration.
This value, combined with the native resolution of the print cartridge of 75, necessitates a DPI of $(12 + 1) * 75 = 975$ in the Y-axis, as the printhead must make at least as many passes as the value of the step size. From this value, the DPI in the X-axis was iteratively tuned, where a value of 2000 gave the best balance between print quality and print speed.
With these values, the print quality was deemed sufficient, and thus the quality factor was left at 1 to not unnecessarily increase print durations.

5.4.2. UV curing

In the LP50 printer that was used for this report, a stationary UV light (Phoseon FireEdge FE300) is present for irradiating the print-platform.
Even though the light from this lamp is collimated into a mostly parallel beam, stray reflections from this light are inevitable and may reach the printhead when it is positioned over the substrate. In order to prevent accidental curing of resin on the printhead, the printhead is moved away from the UV-light to a positioned called the *service position*, and lowered to the lower *Z*-limit. In this position there is no direct path from the light reflected on the print-bed to the printhead.

To move the printhead to this position, however, takes a non-insignificant amount of time, and therefore the decision is made to only cure the deposited material after a full layer is printed. This means that deposited droplets remain in a liquid state for the duration that it takes to finish the printing of the layer, which can take up to several minutes. During this time, the liquid resin can 'bleed' out of the printed pattern, the effect of which is most significant in areas that are printed first and thus remain in a liquid state the longest. To counteract this problem, a small UV-light was constructed that can be mounted directly on the printhead, next to the print-cartridge. This allows for the curing of droplets directly after they are deposited, significantly improving the accuracy of printed patterns.

5.4.3. Print acceleration

In the standard configuration of the Pixdro LP50, the scanning direction is the Y-axis, which is the axis in which the printbed moves.
For each change of movement of the build-plate, an acceleration is required, which imposes an inertial force on both the print-bed and the object that is being printed. This force contributes to the bleeding effect, as it may cause a printed pattern to deform while it is still in liquid form.
This effect is mainly observed in features in the X-axis, perpendicular to the scanning direction, where significant detail is lost, an example of which can be seen in Figure 5.4c. To reduce this effect, the default Y-axis acceleration is lowered from $1500mm/s$ to $700m/s$. This significantly reduces the bleeding effect, as can be observed in the sample in Figure 5.4b which was printed at the lower acceleration.

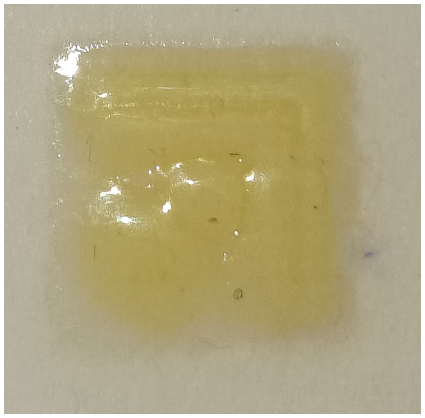
5.4.4. Substrate

The jetted material is deposited on a substrate, and the nature of this substrate may have effects on the quality of the print. Several different substrates have been tested. These include paper, glass, and polyimide tape.

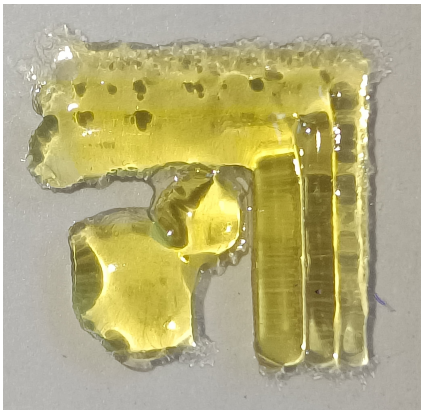
Regular paper is highly porous, typically for the purpose of quickly absorbing water-based inkjet inks. This, however, gives issues when printing a UV-based ink, as the paper partially absorbs the resin but doesn't allow it to cure due to the paper blocking most of the UV light. This effect causes the top layer of the resin to cure, but leaves uncured resin in the paper, giving poor results for the first layers. Additionally, the absorption of resin into the paper reduces the sharpness of printed patterns, resulting in a pattern that looks diffused compared to the original design.

Glass is a hard and non-porous surface, allowing the printed resin to form clean droplets on the glass surface, and to form smooth layers when printed at a sufficient DPI. An effect that was observed was that the glass slides used were slightly contaminated with a residue that caused the printed resin to bead up. After cleaning the glass substrate with IPA, this effect was no longer observed. As the glass is orders of magnitude stiffer than the printed resin, the printed samples can only be removed by forcefully pushing them off the glass, which can be difficult and may result in damage or deformation of the printed sample.

To aid in removing the samples, polyimide tape was used as an alternative substrate. Polyimide is a highly temperature-resistant polymer and is known to withstand the conditions seen in UV sintering. Furthermore, it is non-porous, allowing the deposition of clean and uniform layers.
Adhesion of the cured photopolymer to the polyimide was found to be sufficient, as the parts remain firmly attached to the substrate during printing. After printing, if the sample is desired to be removed from the substrate, the polyimide tape is peeled off, with no damage to the printed samples.



(a) Test pattern printed on regular printer paper at 100 layers. The resin is partially absorbed into the paper, resulting in poor print-quality.



(b) Test pattern printed on a glass microscope-slide at 100 layers. Although bleeding still occurs, significantly more detail is retained.

Figure 5.3: Test-prints printed with the same parameters, but on a paper and glass substrate, illustrating how the porosity of the substrate influences the final result.

5.5. Results

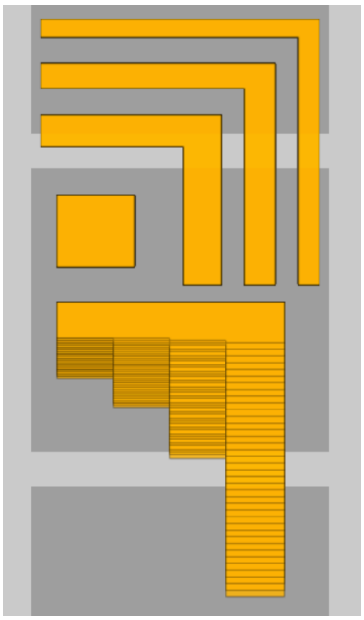
To characterize the geometries and resolutions that can be achieved with the chosen material, several test-prints have been performed. These tests were performed during the tuning-process of the print-parameters, and are documented in chronological order in this section. In subsection 5.5.1, a model is printed with slopes and lines, and the effect of the printer acceleration is visualized. In subsection 5.5.2, the achievable wall steepness, without using the printhead-mounted UV-module, is determined, and the effect of the step size is analyzed. Finally, in subsection 5.5.3, the previous test is again performed, but this time with steeper slopes and while making use of the UV-module.

5.5.1. Ramp test

A 3D test-pattern is printed containing slopes of various angles and lines of various widths in both planar axes. Visible in Figure 5.4a is a top and side view of the design, as viewed in the slicer, and after it has been printed.

By measuring the height of the tallest feature and dividing this by the layer count, a layer height of $5.5\mu m$ is determined. At slopes of high angles, such as the vertical walls in the line segments, a tapering effect occurs which reduces the slope of the wall in the printed object. As the lines get thinner, more material is 'wasted' on this tapering effect, which reduces the final height of the line, which is most noticeable in the upper, thinnest, line. This effect can be attributed to resin bleeding due to it being scanned back and forth whilst in a liquid state, causing it to spread in the scanning direction. In Figure 5.4c, the scanning acceleration was set to $1500mm/s^2$, and more spreading is visible than in Figure 5.4b, where the acceleration was set to $700mm/s^2$. In the line segments printed parallel to the scanning direction, significantly more detail is retained, as the spreading effect is in the same axis as the line.

In the side view, a bulging effect is visible at the top surfaces, where a flat surface is present in the CAD design. This effect is commonly observed in Inkjet 3D-printing, as surface tension forces are present in the layers of deposited resin before they are cured. This pulls especially on the edges and corners of the printed patterns, resulting in a slight rounding effect.
As more layers are stacked on top of each other, this effect accumulates, heavily distorting the top surfaces of tall parts.



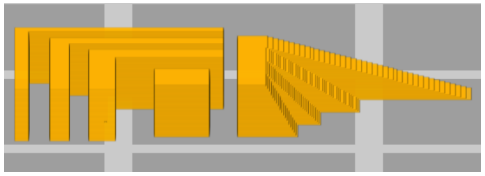
(a) Top view of the sliced benchmark-model, containing lines in the X- and Y-axis of varying width, slopes ad various angles, and a cube.



(b) Printed results of the full benchmark model (500 layers), printed at $700mm/s^2$.



(c) Printed results of half the benchmark model (250 layers), printed at $1500mm/s^2$.



(d) Side view of the test model, as seen in the slicer



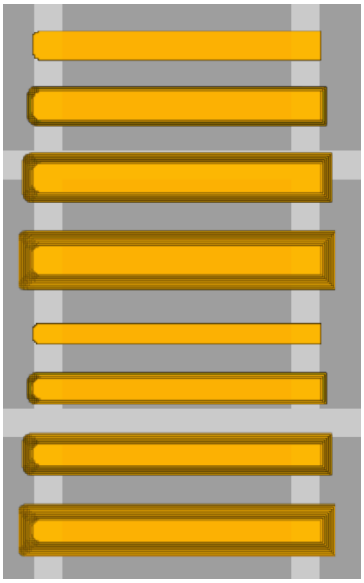
(e) Side view of the printed model, significant bulging is visible at top surfaces, and a height reduction is visible at the thinner lines.

Figure 5.4: Comparison between the 3D model of the test-design, and the model after it has been Inkjet-3D-printed

5.5.2. Line test

A similar test-model is designed with 2 sets of lines, one of 1.5mm wide and one of 2mm, with tapering angles ranging from $90°$ to $75°$.
Visible in Figure 5.5 are the 3D-views of the test design, and the printed results.
In Figure 5.5b, the model has been printed with the step size parameter set to 1; The effect of the variations of individual nozzles can be seen as a wave-like pattern in the X-axis, with a periodicity equal to the total length of the nozzle array $(4.06mm)$. In Figure 5.5c, the same test is repeated, but with a step size set to 12. Now, the effect of variations in nozzle jetting is significantly reduced, as the large wave pattern is no longer visible. Instead, it is now present as a minor stripe-like pattern, with a periodicity equal to the distance between nozzles, $0.34mm$.

Furthermore, a tapering effect is again visible, which is especially present in the lines printed with vertical walls. As the walls in the original design become more tapered, the deviation between the design and the print becomes less significant, until at $70°$, the tapering in the printed model is no more than in the original design.
This natural tapering also causes a height-reduction of the printed lines as more material is 'wasted' on the tapering, which again is more prominent at the thinner lines and reduces as the line width and designed tapering increases.



(a) Top-view of the sliced model of the line test



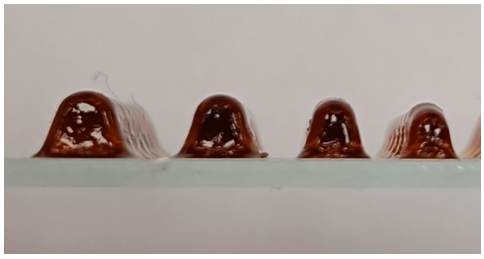
(b) Top view of the printed model of the line test, printed with a step size of 1. A wave-like pattern is present due to jetting variations between nozzles.



(c) Top view of the printed model of the line test, printed with a step size of 12. A repeating pattern can still be seen, but it is significantly less.



(d) Side view of a section of the line test design, containing lines with taper angles ranging from 90° to 70°



(e) Side view of a section of the printed test model. Lines with a slope closer to vertical are naturally tapered and printed less high.

Figure 5.5: Side view of the printed line test model. A tapering is visible in lines even where no taper was designed, and a reduction in height is present in thinner lines.

5.5.3. Aspect ratio test

To characterize the quality improvement gained from using the printhead-mounted UV-module, a model similar to the previous line test is printed but with a higher aspect ratio. In Figure 5.6, a side view of the test model is presented, together with the printed results.

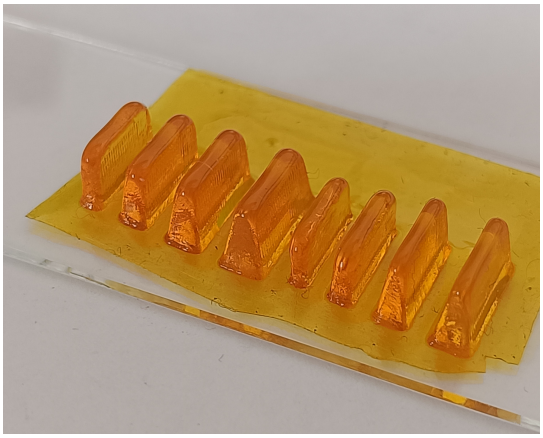
Again, the effect is observed where lines with steeper slope angles are reduced in height, due to resin drooping of the walls. The degree to which this happens is however drastically decreased, and is no longer visible for slopes below 83°. The natural tapering that was observed in previous tests is also significantly reduced, as the resin solidifies before it has the time to droop of the walls. Interestingly, in the thinnest line with a near vertical slope, the resultant print has a overhanging shape, which is hypothesized to be caused by resin drooping of the walls but curing before it reaches the bottom.



Side view, note the overhanging shape visible in center-right line.



Side view of the aspect ratio test in the slicer. The wall slopes range from 80° to 90°.



Angled view of the aspect ratio test

Figure 5.6: Test model for characterizing high aspect-ratio shapes printed with the printhead-mounted UV-module

5.5.4. Design rules

From the aforementioned tests, a set of design rules is formulated to get consistent printed results and minimize the loss of detail. These design rules can serve as guidelines when designing components that are to be printed with the current setup and materials, and have been applied for the components printed in later tests in this report. The design rules are stated as follows:

- Maintain a minimum line width of $2mm$ for lines perpendicular to the scan direction
- Taper vertical walls to 83°
- Avoid sharp corners in layers, by filleting corners

A list with the final printing parameters can be seen in Appendix C.

6

Conductor inkjet printing

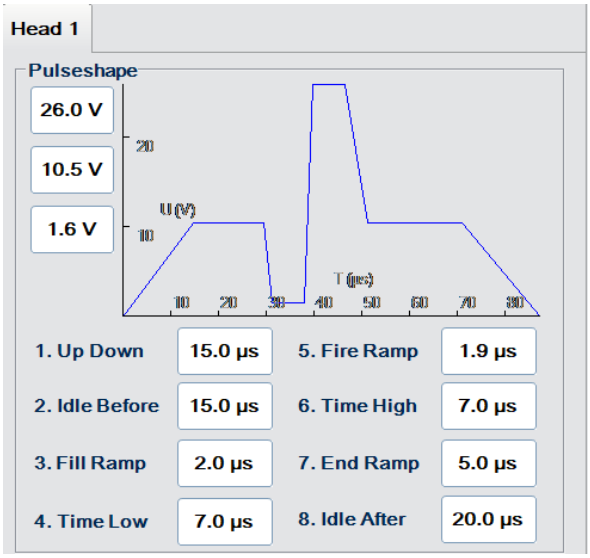
In this chapter, the printing of a conductive material is explored, namely a silver nanoparticle ink (AGNP ink). In section 6.1, the brand and type of AGNP ink are selected, and the rationale is explained. The jetting parameters are described in section 6.2. Next, the process parameters used for UV sintering are explained in subsection 6.3.2, and the DPI tuning process and substrate surface treatment steps are described in subsection 6.3.3 and subsection 6.3.4 accordingly. Several test-patterns are printed to quantify the performance of this setup and can be viewed in section 6.4

6.1. Ink selection

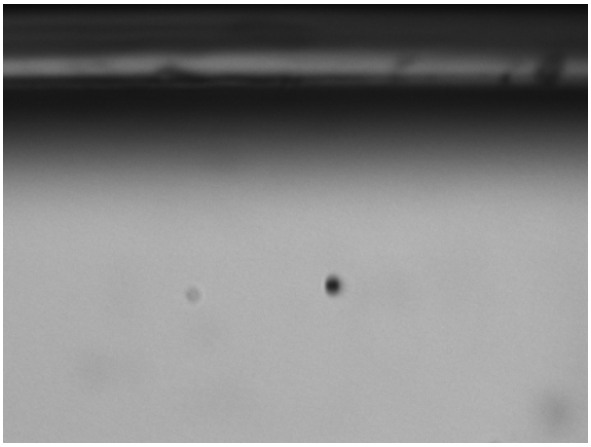
A variety of different types of AGNP inks is commercially available, and have been discussed in Table 2.2. The main differences between these are the carrier liquid, which can either be water-based, alcohol-based, or an organic compound. Additionally, the amount of dispersed silver may vary from 20% to 60% by weight, and various additives may be present to improve wetting.
It was chosen to use NovaCentrix Metallon JS-A211, as it is suited for printing on untreated polymer substrates and was conveniently available in the lab. It is a water-based ink loaded with 40% silver nanoparticles by weight, and contains a fluoropolymer binder for improved wetting. [17]

6.2. Jetting parameters

The printer cartridge used for jetting the AGNP ink is the DMC materials cartridge. This cartridge differs from the DMC Samba in that it has a larger droplet volume, at 10pL, and uses a continuous waveform instead of several separate pulses.
The waveform used was taken from prior literature [6], and can be seen in Figure 6.1a



(a) Waveform used for jetting the AGNP ink



(b) Resultant droplets with one nozzle enabled, as visible in the Pixdro HMI dropview analysis

Figure 6.1: Jetting parameters used for printing NovaCentrix Metallon JS-A211 with the Dimatix 1006 cartridge

6.3. Process parameters

Several aspects of the printing process can be tuned; subsection 6.3.1 describes the parameters used in the motion generator. In subsection 6.3.2, the strategy used for sintering is explained. In subsection 6.3.3, the DPI tuning process is explained, and in subsection 6.3.4 the effect of the substrate on this is explored.

6.3.1. Quality factor & step size

As described in section 5.4, the main printing parameters that can be varied are the dots per inch, the quality factor, and the step size. As the printhead nozzles were found to be much more prone to clogging when using the AGNP ink, and since relatively few layers of conductive material were necessary, the decision was made to select the most reliable nozzle and use only that for printing. As the values for the quality factor and step size are limited to the number of nozzles, their value was fixed to 1.

6.3.2. Sintering parameters

Nanoparticle inks can be sintered through several methods; Chemical sintering, thermal sintering, and photonic sintering are the most commonly used methods, and are further discussed in subsection 2.2.2. For this research, the method of UV sintering is deemed as the most advantageous, for the following two reasons: A powerful UV-light is already present in the printer; thus no extra hardware is needed, and this also allows for sintering without moving the printed sample; thus, no re-alignment is required.

Two strategies of sintering were tested: slowly scanning the UV light over the sample in a single pass, and quickly scanning the UV light over the sample in multiple passes.
When quickly scanning in multiple passes, it was found that the UV light itself was not powerful enough to fully sinter the printed layer, as the silver cools down inbetween passes. This leaves the larger areas of silver unsintered. A method to resolve this is by heating the buildplate to $60°C$, which lowers the required power to achieve sintering conditions. Scanning at full UV intensity at $1mm/s$, with the buildplate heated, sintering occurs in 20 passes.
This method is inconvenient, however, when printing multiple layers, as after sintering the printhead needs to move over the buildplate again. If the buildplate is then still significantly warm, heat radiating from the buildplate heats up the printhead, which lowers the viscosity of the ink and can cause clogs in nanoparticle inks. Due to this, a severe decrease in nozzle reliability and jetting quality was observed when printing over a heated buildplate.
As the buildplate is constructed from a solid piece of aluminum, it has significant thermal mass and can

take over an hour to cool down to ambient temperature, which would drastically increase print duration. For this reason it was opted to perform sintering through only UV irradiation, by means of slowly scanning over the printed pattern in a single pass. Scanning at full UV intensity at $0.05mm/s$, sintering occurs in a single pass.

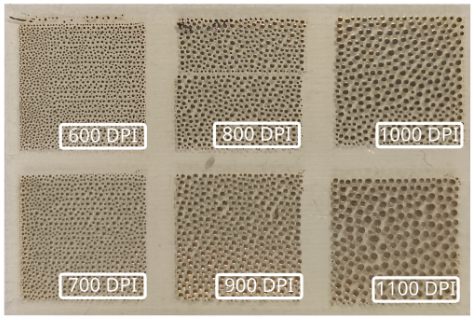
6.3.3. DPI calibration

To achieve a uniform layer of deposited material, the DPI must be carefully tuned. As the substrate material is non-porous and hydrophobic, a DPI that is too low will result in the AGNP ink beading up, as the surface tension prevents the AGNP from forming a uniform layer. If the DPI is set too high, the surface tension is not strong enough to constrain the ink to the printed pattern, resulting in overflowing and loss of detail. Shown in Figure 6.2b are the results of the tuning process, where the DPI is iteratively raised until a uniform printed layer is achieved. It can be seen that in cases with a low DPI, the ink beads up into patches. This effect decreases when raising the DPI, until it is no longer present at a DPI of 1000. Furthermore, the effect of nozzle variations can be seen; two sets of squares printed at 1000 & 1100 DPI by two different nozzles can be seen. Although these are printed with the same DPI and jetting settings, significantly less material is deposited in the left set of squares, which results in more beading. In the right set, a different nozzle was used which was able to deposited more material, giving a uniform layer of silver.

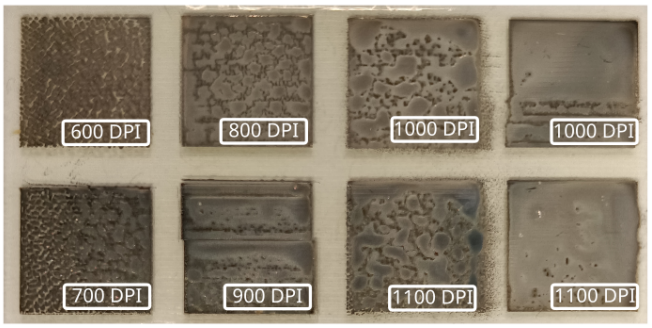
6.3.4. Substrate treatment

When printing AGNP ink on a TPGDA layer which is cured with the standard cure settings, stated in Appendix C, significant beading of the ink occurs. This indicates that even after UV curing, the top surface of the printed polymer is hydrophobic.
The likely explanation for this is oxygen inhibition, which prevents full curing of the top-most layer of the TPGDA and results in a thin film of semi-cured resin on the outer surface of the printed polymer.

To counteract this effect, it was tested to overcure the substrate layer by curing it for a duration that is 20 times longer than the regular curing step.
This significantly reduces the beading when printing the AGNP on top, and allows the printing of a uniform layer of silver. In Figure 6.2a and Figure 6.2b, the difference in beading when printing on normally cured TPGDA vs overcured TPGDA, for different DPI values.



(a) AGNP on normally cured TPGDA with DPI varying from 600 to 1100



(b) AGNP on overcured TPGDA with DPI varying from 600 to 1100. The tests with a DPI of 1000 and 1100 are repeated with a better-functioning nozzle.

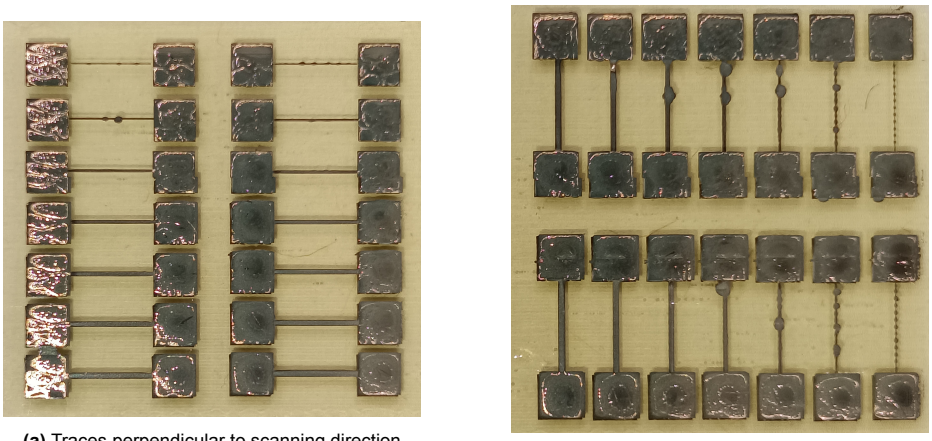
Figure 6.2: Test-patterns printed in AGNP on a TPGDA substrate, illustrating the DPI tuning process, and the effect that the cure duration of the TPGDA substrate has.

6.4. Print Results

To characterize the achievable resolution of this printing process, a resolution test is performed in subsection 6.4.1. In subsection 6.4.2, the conductivity of the printed material is determined by means of a four probe test.

6.4.1. Resolution test

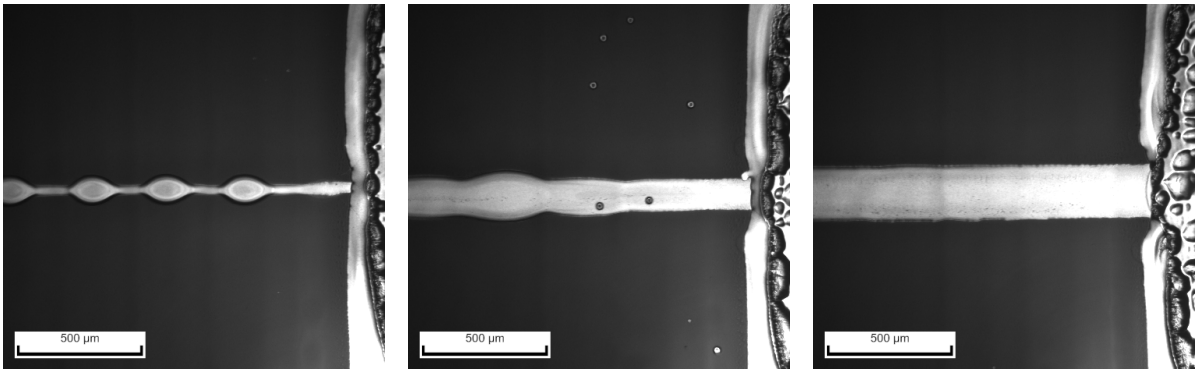
With inkjet printing, the finest resolution that can theoretically be achieved is equal to the size of a single droplet. When printing at 1000 DPI, this comes down to a value of $0.0254mm$.
Circuit traces printed with this width are, however, very susceptible to minor variances in the deposition of the droplets, as even a single misplaced droplet could result in an open circuit. To measure the resolution that can be realistically achieved, a test pattern is printed that contains traces with a width varying from 1 droplet to 14 droplets ($0.0254mm - 0.356mm$), both parallel and perpendicular to the scan direction, on a TPGDA substrate. At each end of the trace a $2mm$ pad is positioned, making it possible to measure if the trace is discontinuous. Visible in Figure 6.3 and Figure 6.4 are the printed test pattern and microscope views of the traces; the measured continuities are reported in Table 6.1.



(a) Traces perpendicular to scanning direction

(b) Traces parallel to scanning direction

Figure 6.3: Resolution test for determining achievable trace widths. Single silver layer printed on 10 TPGDA layers.



(a) Sintered AGNP trace, 1 droplet wide

(b) Sintered AGNP trace, 5 droplets wide

(c) Sintered AGNP trace, 9 droplets wide

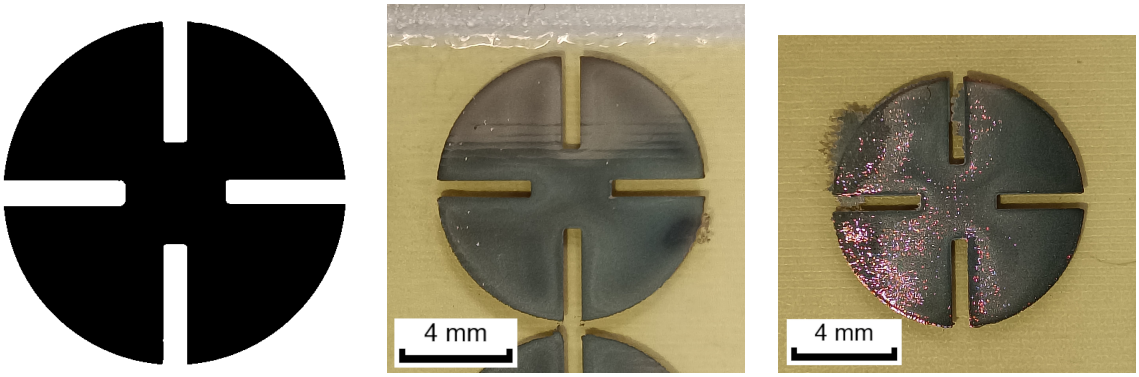
Figure 6.4: Circuit traces printed at different widths; Severe beading is visible at small widths, which decreases for wider traces.

At the thinnest traces, significant inconsistencies in width can be observed, as the ink beads into larger, regularly spaced drops. This effect is most prominent for the traces that are printed perpendicular to the scan direction, where the spacing between these drops is consistently measured to be $0.34mm$. This value is equal to the periodicity of the artifacts seen in Figure 5.5c, which is equal to the spacing between the nozzles of the DMC Samba cartridge. This indicates that the surface of the printed TPGDA is not smooth but rather has micrometer-scale ridges and valleys that affect the deposition of the AGNP

ink.
Furthermore, at the section where the trace meets the larger pad, a necking-like effect is present, resulting in the internal angle of the corner being smaller than the designed $90°$. These 2 effects contribute to thinning segments of the printed traces, which is sufficient to introduce discontinuities in the thinner traces. For wider traces, these variances in width are not sufficient to cause open circuits, resulting in stable traces after exceeding a width of $\sim 0.3mm$.
A proposed improvement is to introduce fillets to the sharp internal corners, to provide a smooth transition to from the thin traces to the wider pads, to counteract the necking-like effect. Additionally, multiple layers of silver could be printed to average out inconsistencies.

Table 6.1: Continuity and resistivity measurements performed on the resolution test. OC indicates an open circuit.

Trace width (droplets)	Trace width [μm]	Resistance [Ω] (perpendicular to scan)	Resistance [Ω] (parallel to scan)
1	23	OC	OC
2	46	OC	OC
3	69	OC	OC
4	92	OC	OC
5	115	OC	OC
6	139	OC	OC
7	162	OC	OC
8	185	73.9	31.4
9	208	OC	OC
10	231	84.5	20.0
11	254	OC	46.1
12	277	16.8	15.9
13	300	57.5	31.5
14	323	16.7	12.8



(a) Cloverleaf pattern for Van der Pauw measurement

(b) Cloverleaf printed in 1 layer of AGNP at 1000 DPI

(c) Cloverleaf printed in 4 layers of AGNP at 1000 DPI. Slight bleeding is visible, which started during the printing of layer 3

Figure 6.5: Printed test-patterns for performing a four-probe resistivity test

Table 6.2: Measured voltage drops and derived sheet resistances of the printed cloverleaf patterns, at a constant current of $1A$

Layer count	$\Delta V_y[V]$	$\Delta V_x[V]$	$R_s[\Omega]$
1	0.046	0.047	0.21
2	0.033	0.036	0.16
4	0.017	0.014	0.070

6.4.2. Conductivity

To validate the conductive properties of the printed silver, a set of cloverleaf test-patterns is printed on a TPGDA substrate, in order to perform a four-probe resistivity measurement using the Van der Pauw method.

These patterns are printed in 1, 2, and 4 layers of silver, and sintered in a single scanning pass. Visible in Figure 6.5a is the test pattern and the resulted printed pattern. On these patterns, a constant current source of 1A is connected to two adjacent pads, and the resultant voltage drop is measured on the two opposing pads. This measurement is performed in both the X and Y axes, resulting in the values presented in Table 6.2. The difference in voltage drops between axis is deemed sufficiently small to assume isotropic conductivity. Next, the average voltage drop is calculated for each test, with which the sheet resistance is calculated according to Equation 6.1.

$$R_s = \frac{\pi R_{avg}}{\ln 2} = \frac{\pi V_{avg}}{I \ln 2} \tag{6.1}$$

As expected, the sheet resistance is the highest for a single layer of printed silver, and decreases when stacking multiple layers until a sheet resistance of $70m\Omega$ is calculated for the case of 4 stacked layers.

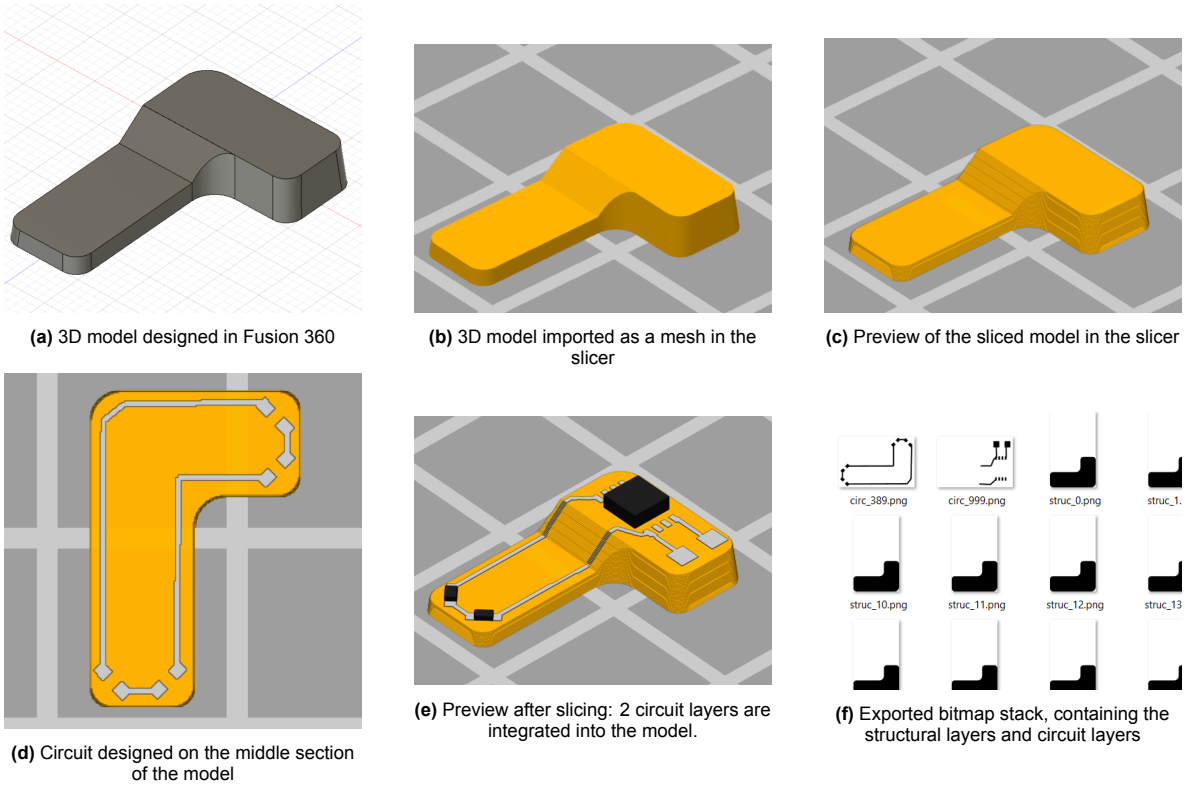
7

Structural electronics printing

To 3D-print structural electronics, at least two materials are required: a structural material that acts as an insulator, and a conductive material that serves to carry electric current. Additional materials may be included in the process and include support material, actuating materials, ferromagnetic materials, semiconductor materials, etc. To limit the scope of this thesis, only the combination of insulator and conductor is investigated.
The print settings for these materials have been separately tuned in chapter 5 and chapter 6. In this chapter, the slicing algorithms that have been described in chapter 4 are validated through the process of test-printing, in which the TPGDA resin and AGNP ink are combined to print examples of structural electronics.
section 7.1 explains the software workflow which is used to transform a parametric design into a format that can be printed on the Pixdro LP50. section 7.2 explains the (manual) steps involved to enable the printer to print the processed files. Then, in section 7.3, a selection of test models is fabricated with the purpose of demonstrating the design features in the developed slicer.

7.1. Software Workflow

Similar to the conventional 3D-printing process, the first software application used in this process is a CAD program. In this report, Fusion 360 is used for this purpose, as it is a convenient tool for designing parts for additive manufacturing and rapid prototyping.
In the CAD program, a 3D solid is designed, an example of which can be seen in Figure 7.1a, which is then exported as an STL mesh file. This file is imported in the slicer, where a view such as Figure 7.1b is then presented. Then, the model is centered and sliced, resulting in a layer-based view, as can be seen in Figure 7.1c.
Next, circuit layers are added at the desired layers, which may include vias, electronic components, and (air-exposed) pads. After the circuits are designed, the model is sliced again, which integrates the circuits into and onto the 3D solid, according to the algorithms described in chapter 4. Finally, the model is exported, which renders the structural layers and circuit layers at the highest resolution and saves them into a folder.



(a) 3D model designed in Fusion 360

(b) 3D model imported as a mesh in the slicer

(c) Preview of the sliced model in the slicer

(d) Circuit designed on the middle section of the model

(e) Preview after slicing: 2 circuit layers are integrated into the model.

(f) Exported bitmap stack, containing the structural layers and circuit layers

Figure 7.1: Slicer software workflow, showcasing how a model is first designed in a CAD-program, then processed in the slicer, and finally exported as a bitmap stack.

7.2. Printing workflow

With the model sliced into a bitmap format, it can be transferred to the PC connected to the Pixdro printer. In the Pixdro HMI, the 3D-printing recipe is enabled and the correct files are selected.
For printing the structural material, the printing parameters explored in chapter 5 are used, and for the AGNP ink, the parameters from chapter 6. Due to only having one DMC Samba HPB and one DMC HPB available, it was not possible to load the 2 materials simultaneously, and thus manual material switching was required.
Before printing, the substrate must be prepared, for which glass slides covered in polyimide tape are used. These are positioned on the build-platform with a 3D-printed alignment tool, and taped down with painter's tape. To reduce beading of the first layers of structural material, the substrate is cleaned with IPA, after which the print can be started.

It is preferred to not move the glass slide in between print-jobs, so as to prevent misalignments between layers. However, this can't be avoided when electronic components are to be soldered onto the circuit. In this case, the slide can be re-aligned making use of the same 3D-printed alignment tool.

After printing, the slide can be easily removed from the build-platform by peeling off the painter's tape. If the printed sample needs to be detached from the slide, this can be done by carefully peeling off the Kapton from the glass slide, during which the printed object typically pops off the substrate by itself.

7.3. Results

Several features have been developed in the slicer specifically for the purpose of fabricating structural electronics parts. In subsection 7.3.1, the process of embedding (non-planar) circuits into a solid of structural material is tested. In subsection 7.3.2, the dimple vias, which are generated in the slicer, are printed and tested. subsection 7.3.3 describes the process of bonding electronic components to printed pads. Next, the process of embedding these bonded components in structural material is explored in subsection 7.3.4. Finally, a strategy for producing air-exposed pads is tested in subsection 7.3.5

7.3.1. Circuit overprinting

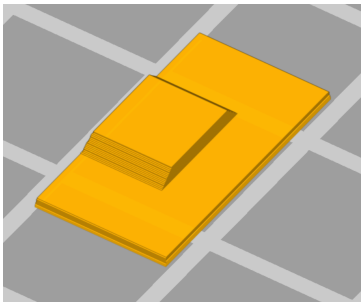
To test the capabilities of embedding circuits in the structural material, a test object is fabricated containing a 2.5D circuit over which a structure of polymer is printed. The part is sliced using the 'sandwich slicing' mode in the developed slicer, and is comprised of two 3D models, with the circuit embedded in-between.
Visible in Figure 7.2 are the 3D previews of the model generated in the slicer and the printed results.
The fabrication steps for this component were as follows:

1. A glass slide was covered with Kapton tape and fixed in place.
2. The print cartridge was loaded with photoresin.
3. The first segment was printed using the photoresin.
4. The cartridge was swapped with one containing AGNP (silver nanoparticle) ink.
5. Circuit patterns were printed onto the cured TPGDA surface.
6. The printed circuit was sintered using high-intensity UV light.
7. The cartridge was switched back to photoresin.
8. The lower portion of the second segment was printed with a layer height set to 0, allowing contact with the embedded layer.
9. The upper part of the second segment was printed using standard parameters.

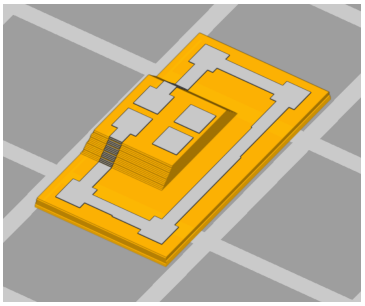
During the overprinting step, where resin was deposited on the previously printed and sintered circuit traces, no noticeable difference in deposition behavior between the resin and the silver was observed compared to the deposition of resin on cured resin.
However, significant warping was observed in the final printed sample (see warp) This deformation is attributed primarily to the sintering step, during which uneven heating from high-intensity UV exposure occurred. The warping effect was likely exacerbated due to the sample being removed from the polyimide substrate after printing the first segment, as the sample was no longer constrained from curling up.
The embedded circuit was printed in three stacked layers. Its layout connects two upper contact pads via a trace that follows the component's perimeter, including two $45°$ ramps. Electrical resistance measurements confirmed continuity, yielding a total resistance of $23, \Omega$.

7.3.2. Via test

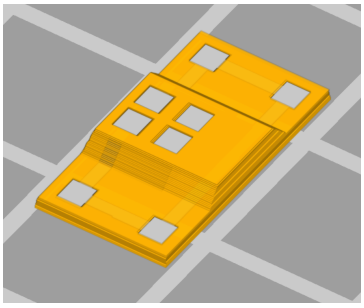
To validate the principles of the vias explained in subsection 4.2.7, a test was conducted in which a set of vias was printed with varying heights.
Two types of vias can be generated in the slicer software: dimple vias and stairwell vias. Stairwell vias require multiple manual interventions during printing, as each step involves both resin and AGNP ink. Due to the necessity of manually switching the printer cartridge when changing materials, stairwell vias are not practical for this test.
Therefore, only dimple vias were evaluated, as they can be fabricated in just four steps. The test structure, as illustrated in Figure 7.3a, includes vias with heights of 0.3 mm, 0.6 mm, and 0.9 mm. The corresponding print results are shown in Figure 7.3b, and the measured resistances of the resulting circuits are presented in Table 7.1. The initial test was performed with vias with a bottom hole diameter of 1.1 mm, and resulted in most vias not connecting through. The test was repeated with a larger hole diameter, 1.6 mm, and resulted in all vias connecting through.
It is hypothesized that, in the original test, a small amount of uncured resin may have drooped along the sidewalls of the via, ultimately covering the lower contact pad and preventing electrical connection with the top circuit. An alternative explanation is that partially clogged or degraded nozzles in the printhead cartridge deposited small amounts of resin unintentionally. This unintentionally deposited resin can form a thin film covering up the lower contacts of the via.



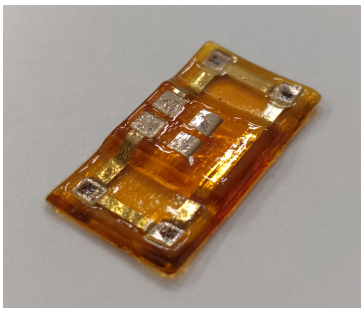
(a) Sliced preview of the primary structure of the model.



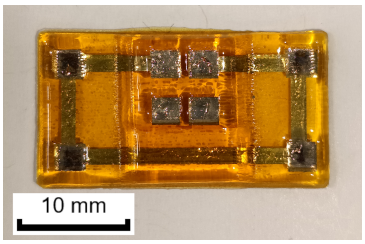
(b) Sliced preview of the lower section of the model with a non-planar circuit layer on top



(c) Full sliced preview of the designed model. A secondary structure is printed over the primary structure and circuit.

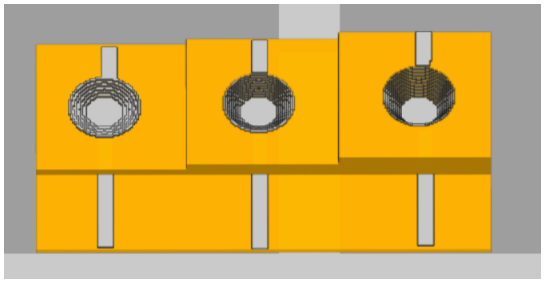


(d) Printed result of the designed model. Significant warping is visible on the bottom surface.

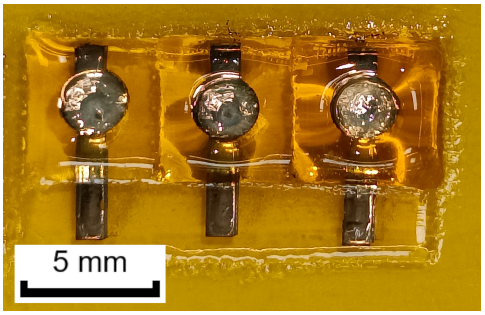


(e) Top view of the printer model, showing how the circuit can be seen through the semi-transparent structure.

Figure 7.2: Design and results of a model with an embedded circuit and exposed pads.



(a) Test-model containing 3 dimples, spanning heights of $0.3mm$, $0.6mm$, and $0.9mm$



(b) Printed result of the test-model, containing 3 dimple-vias

Figure 7.3: Dimple vias as designed in the slicer and after printing

Table 7.1: Measured via resistance, OC indicates an open circuit

Via height / Hole diameter	**0.3mm**	**0.6mm**	**0.9mm**
1.1mm	14.6Ω	OC	OC
1.6mm	0.4Ω	0.9Ω	0.5Ω

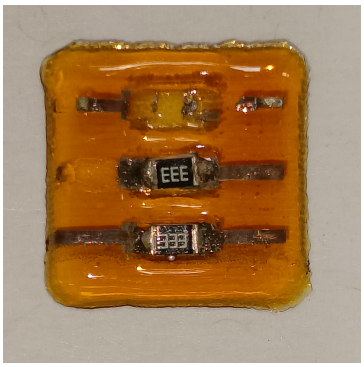
7.3.3. Component bonding

The bonding of electronic components makes it possible to add active functionality to the printed circuits. These components range from simple elements such as light-emitting diodes (LEDs) and resistors to more complex devices like microprocessors and connectors.

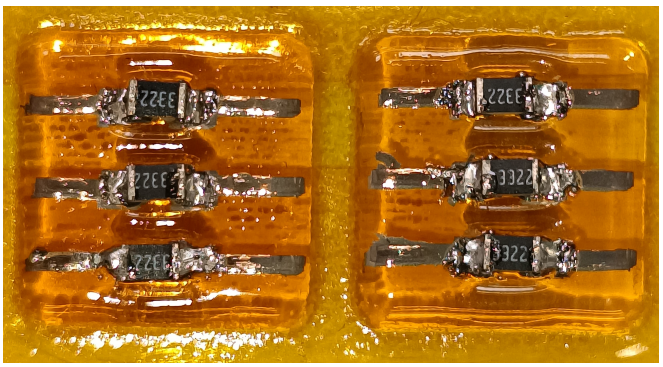
To establish an electrical connection between a component and the circuit, galvanic contact must be made between the contact pads of the component and the printed circuit pads. Several bonding strategies have been demonstrated in the literature, including:

- Soldering (including solder paste)
- Conductive epoxy
- overprinting with AGNP ink

Soldering is the most widely employed bonding method in electronics fabrication, as it is a cheap and consistent process that results in reliable bonds. It does, however, come with elevated temperatures, as it necessitates the melting of the soldering material, which can possibly result in degradation of the polymer material or the silver layer.
To test the viability of soldering components to the printed circuits, a test pattern is created containing pads onto which 0805 SMD resistors can be soldered. The test-pattern is designed for bonding 3 0805 resistors, and a cavity is present in the structural material into which the components can be placed. As the inkjet printing process results in slightly undersized holes, the holes in the design are slightly oversized, allowing a loose fit.
Following the printing and sintering process, the printed structures were removed from the printer. Solder paste, ChipQuick TS391LT10, was manually applied to the pads. Subsequently, 0805 resistors were manually positioned within the cavities. The pads were then heated using a hot air gun set to $325°C$ until the solder paste melted and established an electrical and mechanical bond with the components.
Visible in Figure 7.4 are the results of the printed circuits with the soldered components. During the soldering process, no degradation of the structural material was observed, which concurs with the degradation temperature of TPGDA being reported to be $300 - 400°C$ [14].
Severe degradation of the printed silver pads and traces is clearly visible in Figure 7.4a. This phenomenon, where the silver delaminates from the substrate and is absorbed into the molten solder, is known as leaching and is caused by the natural tendency of silver to dissolve in molten solder. Leaching is a well-documented issue in cases where AGNP ink is printed on smooth, polymer substrates. [40] [38] In the literature, several methods have been reported to reduce the effect of leaching, which include printing multiple layers of AGNP ink, sintering the AGNP for longer at higher temperatures, and using solder paste containing a small fraction of silver.
In Figure 7.4b, the soldering test has been repeated, but on samples containing 6 layers of printed silver. This stacking of layers results in a significantly more robust silver layer, and no degradation due to leaching is visible after the soldering step. Continuity tests with a digital multimeter indicate the components are fully connected, with the majority of the resistance in the circuit being ascribed to the resistors.



(a) Printed sample with cavities and pads for soldering 0805 resistors, the circuit is printed in 2 layers. Significant damage has occurred during soldering, due to the leaching effect.



(b) Repetition of the soldering test with 6 layers of printed silver. Only minor leaching has occurred and all resistors are successfully soldered.

Figure 7.4: Samples used for solder-testing, indicating how the number of printed silver layers affects the robustness during soldering.

7.3.4. Component Embedding

A promising aspect of structural electronics is the ability to embed electronic components in the structural matrix. As Inkjet printing is a non-contact additive manufacturing method, it allows printing over a

uneven surface, which may include (electronic) components.
To test this ability, a circuit was printed containing pads for two LEDs and a current-limiting resistor. Additionally, his model contains cavities that have been generated in the slicer, allowing the components to be recessed into the structure. This ensures that the printhead will not collide with the soldered components.
After printing and sintering, the circuit was removed from the printer, and the components were soldered onto the circuit using solder paste. Subsequently, the circuit was repositioned in the printer, and a pattern was printed to fill the remaining cavities with photoresin. To achieve a smooth surface finish, no UV curing was performed immediately after printing, allowing the filler material to flow freely and completely fill the cavities.

Finally, the remaining portion of the model was printed over the circuit using standard printing parameters.



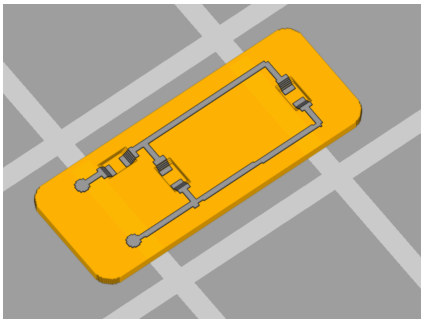
(a) Printed circuit containing a current-limiting resistor and 2 LEDs.



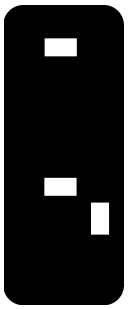
(b) LED circuit overprinted with photoresin, embedding the circuit. Vias to the top surface are present for powering the circuit, but didn't connect all the way through.

Figure 7.5: Sample of a printed LED-circuit, before and after overprinting with photoresin

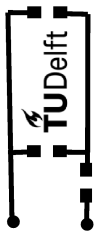
In the printed results, a slight bump is present at the top surface above the embedded components. This indicates one of the challenging aspects of embedding components: The volume and shape of the embedded component must be exactly modeled such that the material filling the cavity is not insufficient or excessive. Additionally, the solder-paste takes up volume as well, which must also be accounted for.



(a) Design of the bottom layer of the LED circuit, showing the circuit traces and cavities for components.



(b) Exported bitmap for printing the lower section of the structural material of the LED circuit.



(c) Exported bitmap for printing the circuit layer, containing pads for the components. The TU Delft logo has been added manually after exporting.

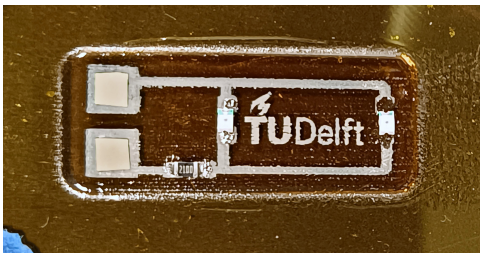


(d) Exported bitmap for filling the remaining cavities around the components with photoresin after soldering.

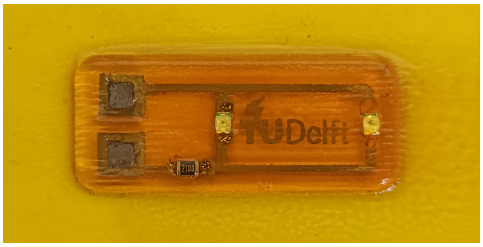
Figure 7.6: Sliced model and exported files used for printing the LED circuit.

7.3.5. Printing exposed pads

Occasionally, a nozzle on the printhead becomes clogged, which may lead to several outcomes: the nozzle can either cease jetting entirely, continue jetting with droplets being ejected at an angle, or jet droplets that do not form correctly.
In the last case, these deformed droplets have been observed to break up during flight, resulting in the misplacement of resin. When printing models with vias or exposed pads, it is essential that no photoresin is deposited on the exposed contacts, as this may compromise the ability of a via to connect two layers or of a pad to be probed.
To counteract this issue, it has been tested to mask the exposed contact pads with a small, manually placed piece of tape. After printing is finished, these are removed, and reveal the uncovered contact pads. Figure 7.7a shows a sample with masked contact pads, and in Figure 7.7b this sample is showcased after printing and removal of the masks.
Alternative approaches to address this problem include the use of more reliable nozzles, employing photoresin formulations that are less prone to droplet break-up during jetting, and implementing automated detection systems for malfunctioning nozzles.



(a) LED circuit during printing. Paper masks are positioned over the pads to shield them from leaking resin.



(b) LED circuit after printing with the paper masks removed, exposing the uncovered pads.

Figure 7.7: Tested method to ensure pads remain clear of photoresin.

8

Discussion

8.1. Slicer

The slicer consists of 3 main components: the structural slicer, the circuit designer, and the circuit slicer.
The structural slicer was developed first, as a tool for generating inkjet-printable bitmaps from STL models, and rendering a 3D preview. Significant attention was given to memory management, as the high resolution of inkjet-3D-printing can result in an excessive amount of volumetric data. The strategy to handle this, by only retaining a single sliced layer in the working memory at once, proved to be successful, and allows the slicing of relatively large models. Furthermore, the decision to use Python allows the program to function on many platforms, and it has even been successfully tested on a Raspberry Pi 4 which offers very limited computing power.

The circuit designer tool was implemented with only the minimum viable functionality. Several quality-of-life features, such as undoing operations and saving and loading designs are currently absent. In addition, features that are present in conventional circuit design software, such as importing circuit diagrams and testing trace continuity, are not implemented, which makes the creation of more complex circuits difficult. Nevertheless, the tool remains a convenient solution for creating simple circuit layouts.

The circuit slicer, responsible for integrating circuit elements into the sliced 3D model, constitutes the most complex part of the slicer algorithm. Since only one sliced layer resides in memory at a time, direct operations on the full 3D volumetric dataset are not feasible. This limitation required several workarounds to enable operations that would be trivial to implement on 3D data, and necessitated the use of several storage buffers, such as for support generation or laying down circuits. This, combined with the iterative development of the slicer, results in the full slicing algorithm being convoluted, and there is significant room for optimization. Despite this, the integration of circuits into 3D models is fully functional, and the program proved to be a very useful tool for the process of inkjet-3D-printing structural electronics.

8.2. Polymer printing

Compared to other inks that have been tested during the course of this study, the TPGDA resin exhibited relatively poor printing performance. The jetted droplets demonstrated a higher tendency to break up during flight, which severely limited the achievable resolution. By positioning the printhead as close as possible to the substrate ($0.5mm$), significantly more detail was achieved, but this may not be possible when printing over non-flat surfaces. Additives which increase the surface tension or the viscosity of the resin may improve this, as may the use of different printheads.

The DMC Samba Materials Cartridge is a platform originally designed for testing new inks, and to tune the printing parameters for using large Samba printheads. The DMC Samba, however, has a very small

number of nozzles, which can eject only a small volume of material each. This makes it not quite suited for 3D printing, as print-times, even for millimeter-scale objects, may exceed 10 hours.
This greatly lengthens iteration cycles, and due to the long time and many passes that it takes to print a single layer, allows the deposited material to spread significantly before being cured.
The use of different printheads may again improve quality in this aspect, and greatly reduce the print-times, as printheads exist which can jet over a thousand times the volume as the DMC Samba.

Overtime, the jetting quality of the nozzles noticeably decreased, as nozzles were produced less consistent droplets and clogged more frequently. It is expected that this is either due to wear of the nozzles, or due to minor amounts of photoresin curing around or in the nozzle openings.

8.3. AGNP printing

The AGNP ink used in this study, NovaCentrix Metallon JS A-211, proved to be compatible with the TPGDA, and could even withstand minor scratching and application and removal of painter's tape.
Soldering to the printed pads, however, proved challenging. While partial success was achieved, the process was inconsistent and required rapid execution. Several potential improvements may be explored in future work. These include increasing the number of printed silver layers to enhance pad robustness, employing higher sintering temperatures, utilizing silver-containing solder pastes, or adopting alternative bonding methods such as conductive epoxy or overprinting with additional AGNP ink.

During sintering, it was noticed that thin features, such as traces and corners, dry and sinter significantly faster than larger solid areas. The exact mechanism behind this was not found, but it may be caused by the heating of the TPGDA under the high-intensity UV light. Further investigation in this aspect may be performed, and advantage of this phenomena could possibly be taken by replacing large solid shapes with a hatched pattern, for significantly faster sintering.

Two cartridges with AGNP ink were used in this report, both filled with NovaCentrix Metallon JS A-211. A significant variance in wetting was noticed between these two, as one ink started bleeding at a DPI as low as 700, whilst the other could be successfully printed at 1100 DPI. It is thought that this might be the result of poor mixing of the fluoropolymer binder, or aging of the ink, and indicates that even minor variations in ink composition can have a major effect on the achievable print quality.

8.4. Structural electronics printing

One significant challenge encountered during the printing of the electronics was the unintended deposition of photoresin on air-exposed pads, which resulted in their insulation. This issue led to via failures and rendered several pads non-functional. This effect becomes more prevalent as the distance between the printhead and the substrate increases, as the jetted droplets have more time to break up or go off path.

Due to hardware limitations, it was not possible to load both the AGNP and photoresin simultaneously. As a result, manual switching between materials was necessary. This constraint significantly limited the complexity of printable designs, as material changes could only be performed during daytime hours, while certain prints required up to 15 hours to complete. Consequently, this made it impractical to test the stairwell via concept, which necessitates frequent material switching over extended periods.

The embedding of electronic components was largely successful; however, slight surface irregularities remained over the embedded parts. Effective embedding requires an accurate 3D model of the component and precise knowledge of the layer height in order to minimize such imperfections.

9

Recommendations

In this chapter, recommendations are made to aid future studies and to inspire further research in this topic

Polymer printing

- As stated in the chapter 8, multiple issues were related to the used printhead. For future research, it is advised to make use of printheads that are capable of ejecting a significantly larger volume and that have an order of magnitude more nozzles.
- Significant vertical bulging effects occur due to surface tension in the liquid photoresin. Commercial Polyjet and Multijet printers utilize a (heated) roller or scraper to ensure a printed layer has exactly the planned height. Utilizing such a system could drastically improve the achievable print accuracy.
- When comparing the used photoresin with inks specifically formulated for inkjet printing, it is observed that the droplets that are formed are less consistent and occasionally break up mid-flight. Additives such as surface tension enhancers could be tested to improve the jetting behavior of the photoresin.

AGNP printing

- It was observed that utilizing a heated build-platform results in quicker drying and sintering of the deposited AGNP ink. However, as the build-platform in the LP50 has significant thermal mass, heat radiates from the build-platform onto the printhead, which both affects the jetting performance and can also cause clogging. To improve this, it could be tested to use a heater with less thermal mass, such as PCB-heater. Additionally, with a PCB-heater, it would be possible to selectively heat only the desired areas.
- Alternatively, for sintering the AGNP ink, even more localized sintering methods could be investigated, such as laser diodes. This would allow to only heat the silver traces, while leaving other areas, such as support structures, unaffected.

Printing hardware

- Several hardware and software malfunctions have occurred during the use of the LP50 printer. Furthermore, the Pixdro HMI and LP50 only allow a limited scope of modifications. As many open-source 3D printing-platforms exist with robust motion systems and well-documented hardware and software, it might be beneficial to investigate the possibilities of modifying existing 3D printers with inkjet hardware, which would significantly reduce the barrier of entry for inkjet-based 3D-printing, and open up possibilities for hardware customization.

Structural electronics printing

- With the current equipment, it was not possible to print both the conductive and structural material simultaneously. This limited the complexity of printed designs, as manual intervention was

required for each material change. Using a multi-material printhead, such as the dual Spectra head, would allow for the automatic printing of significantly more complex designs.

- Although the resolution of inkjet-printed structural electronics is sufficient for many applications, the mechanical properties of jettable photoresins are often lacking. Combining inkjet 3D printing with FDM 3D printing would make it possible to utilize the advantages of both technologies; It would be possible to FDM-print large mechanical parts in a high performance thermoplastic, whilst simultaneously inkjet-printing internal channels or veins with photoresin and AGNP ink, for integrating electronic circuits and sensors.

Software & Slicer

- In the current form, circuits are designed and integrated in the slicer. The benefit of this is that a slicer is a relatively simple program to add such features to, due to the layer-based nature of slicers. It does, however, limit the capability to incorporate existing geometric features of the model into the slicer. For a general-purpose tool, it is deemed to be more convenient to integrate the circuit design and integration into an existing CAD program. Several open-source CAD initiatives exist, such as FreeCAD, which could be a suitable platform for this purpose.
- In this report, the printing of support structures was not tested, although the feature is present in the slicer. When printing a support material, it is likely that the layer height differs from that of the structural material. Therefore it would be recommended to decouple the support and structural layer height in the slicer to compensate for this.
- Conventional PCB design programs typically export the designs in the Gerber format, essentially a vector-based image format. The developed slicer could be modified to enable the importing of Gerber files, and slice them into an inkjet-printable format. This would essentially result in a single-machine PCB-factory, capable of fabricating high-resolution, high layer count PCBs.
- Due to the surface tension of the printed ink, corners of printed patterns are inherently rounded, which results in loss of detail in designs with sharp corners. In regular printing of text on paper, the effect of ink spreading results in a similar loss of detail, which is counteracted by using specialized fonts with so-called ink-traps. A similar technique could be attempted in the process of inkjet-based 3D-printing, by deforming certain geometric features during the slicing process to account for deformations due to surface tension in the printing process.

10

Conclusion

The primary goal of this thesis was to investigate the potential of Inkjet 3D printing for the fabrication of structural electronic components.
In the literature review, it was identified that there is a significant lack of open-source software specifically designed for processing models for inkjet-3D-printing. To address this gap, a custom slicer was developed that converts STL files into a stack of bitmaps suited for inkjet printing. To enable the integration of electronic circuits into 3D-printed structures, several strategies were developed, worked out into algorithms, and incorporated into the slicer. The resulting tool includes a dedicated circuit design mode, allowing users to draw conductive traces and pads, add electronic components, and define vias. These circuits are embedded within the 3D model and exported alongside the structural model as a bitmap stack.

For printing structural electronics, at least a conductive and a structural material are required.
For the structural component of the printing process, a photoresin based on tripropylene glycol diacrylate (TPGDA) was selected. This choice was motivated by its open formulation, high temperature resistance, and prior use in literature. Print parameters for this material were tuned through an iterative process. The strategy chosen for UV-curing the material was to utilize the high-power UV-bar in the LP50 printer to cure after each layer was fully printed. Loss of detail was observed due to the liquid resin spreading before being cured. To counter-act this, a low-power UV light was mounted on the printhead to cure the material directly after depositing, and improved results were observed. A series of benchmark models were fabricated to characterize the achievable accuracy of this process. A line width of $1.5mm$ was could be achieved with good accuracy, and walls with an angle of up to $75°$ could be consistently printed. Nonetheless, bulging artifacts were observed on top surfaces, attributed to surface tension effects in the liquid resin prior to curing.
For the conductive material, NovaCentrix Metallon JS-A211 ink was selected, a silver-nanoparticle ink. Similar to the structural resin, printing parameters were optimized through iterative testing, and the process was characterized through a series of printed test-patterns. The post-processing routine developed for this material consists of UV-sintering by slowly scanning the high-power UV bar over the printed pattern. After sintering, a sheet resistance of 0.21Ω was measured per layer. Additionally, trace widths down to $0.3mm$ could be consistently achieved in all directions.

These 2 materials were combined by printing a series of test models which were prepared in the developed slicer. These tests included a model with a non-planar embedded circuit layer, the printing of via structures, the printing of pads onto which electronic components were soldered, the embedding of components into the structural material, and the printing of air-exposed pads.
The soldering of components to the printed silver pads proved difficult due to an effect identified as leaching, where the silver is absorbed into the molten solder. Printing more robust pads by stacking layers of silver improved results, but pad delamination could not be completely resolved.
Other encountered issues were the covering of vias and pads by non-intentionally deposited resin,

resulting in insulated pads or vias that did not connect. The cause for this issue was attributed to malfunctioning printer nozzles and poor jetting properties of the photoresin.

Several recommendations were made that may significantly improve the achievable quality and consistency of this process for future research.
While challenges remain, inkjet-3D-printing serves as a promising manufacturing method for structural electronics. The process may significantly improve performance in fields where mass or size are limited, and these same processes may be utilized for fabricating printing circuit boards, allowing for cheap and rapid prototyping, and decentralized production.

References

[1] *3D-Printable Electronics-Integration of SMD Placement and Wiring into the Slicing Process for FDM Fabrication*. URL: https://www.researchgate.net/publication/319956919_3D-Printable_Electronics-Integration_of_SMD_Placement_and_Wiring_into_the_Slicing_Process_for_FDM_Fabrication.

[2] *ANP □□□□□*. URL: http://www.anapro.com/en/sub/business/product/product.php?mode=view&idx=17.

[3] Anil Bastola et al. "Formulation of functional materials for inkjet printing: A pathway towards fully 3D printed electronics". In: *Materials Today Electronics* 6 (Dec. 2023), p. 100058. ISSN: 2772-9494. DOI: 10.1016/J.MTELEC.2023.100058.

[4] Patrick W. Cooley, David B. Wallace, and Bogdan V. Antohe. "Applications of ink-jet printing technology to BioMEMS and microfluidic systems</title>". In: *Microfluidics and BioMEMS* 4560 (Sept. 2001), pp. 177–188. DOI: 10.1117/12.443057. URL: https://www.researchgate.net/publication/236686015_Applications_of_Ink-Jet_Printing_Technology_to_BioMEMS_and_Microfluidic_Systems.

[5] V. Correia et al. "Design and fabrication of multilayer inkjet-printed passive components for printed electronics circuit development". In: *Journal of Manufacturing Processes* 31 (Jan. 2018), pp. 364–371. ISSN: 1526-6125. DOI: 10.1016/J.JMAPRO.2017.11.016.

[6] C T Davenne. "Department of Precision and Microsystems Engineering Multi-material 3D inkjet printing for functional structures using UV sintering and photopolymerisation". In: (2021). URL: http://repository.tudelft.nl/..

[7] *Deisgn Guide for PolyJet Additive Manufacturing*. URL: https://support.stratasys.com/SupportCenter/HTML5UserGuides/Design_DFAM_Guide_July_2020/Responsive%20HTML5/DOC-01103_x_Design-PJ-AM-Guide-HTML/DfAM_Guide-Chapter/DfAM_Guide-Chapter.htm.

[8] *Digital Inkjet Solutions for OEM | Sun Chemical*. URL: https://www.sunchemical.com/digital_oem-inkjet-solutions/.

[9] Ahmed Elkaseer et al. "Material jetting for advanced applications: A state-of-the-art review, gaps and future directions". In: *Additive Manufacturing* 60 (Dec. 2022), p. 103270. ISSN: 2214-8604. DOI: 10.1016/J.ADDMA.2022.103270.

[10] *FLIGHT HUB: 3D Printing Software for eCad/mCad integration*. URL: https://www.nano-di.com/resources/blog/flight-hub-additive-manufacturing-of-electronics-electronics-design-software.

[11] *FPM-Trinity*. URL: https://www.fuji.co.jp/en/about/fpm-trinity/.

[12] Björn Gerdes. "StarJet printheads for printing molten solder jets at 320 °C and molten aluminum alloy droplets at 950 °C". In: (2019). DOI: 10.6094/UNIFR/150324.

[13] *Guidance on How To Use the New Samba Cartridge*. URL: https://dimatix-5352080.hs-sites.com/samba-how-to.

[14] Yinfeng He et al. "A Tripropylene Glycol Diacrylate-based Polymeric Support Ink for Material Jetting". In: *Additive Manufacturing* 16 (Aug. 2017), pp. 153–161. ISSN: 2214-8604. DOI: 10.1016/J.ADDMA.2017.06.001.

[15] *How PCB Inkjet Printing is Revolutionizing PCB Fabrication*. URL: https://hilelectronic.com/pcb-inkjet-printing/.

[16] Ian M. Hutchings and Graham D. Martin. "Inkjet Technology for Digital Fabrication". In: *Inkjet Technology for Digital Fabrication* (Nov. 2012), pp. 1–372. DOI: 10.1002/9781118452943. URL: https://onlinelibrary.wiley.com/doi/book/10.1002/9781118452943.

[17] *Inkjet Conductive Inks - NovaCentrix*. URL: https://novacentrix.com/inkjet-conductive-inks/.

[18] *InkOrmo*. URL: https://kayakuam.com/wp-content/uploads/2022/01/PI_InkOrmo.pdf.

[19] Zhiwei Jiao et al. "Experimental research of drop-on-demand droplet jetting 3D printing with molten polymer". In: *Journal of Applied Polymer Science* 135.9 (Mar. 2018). ISSN: 10974628. DOI: 10.1002/APP.45933. URL: https://www.researchgate.net/publication/320843990_Experimental_research_of_drop-on-demand_droplet_jetting_3D_printing_with_molten_polymer_Research_Article.

[20] Do Kyeong Lee et al. "Fabrication of 3D structure with heterogeneous compositions using inkjet printing process". In: *Materials Today Communications* 35 (June 2023), p. 105753. ISSN: 2352-4928. DOI: 10.1016/J.MTCOMM.2023.105753.

[21] Chun Li et al. "Recent Developments of Inkjet-Printed Flexible Energy Storage Devices". In: *Advanced Materials Interfaces* 9.34 (Dec. 2022). ISSN: 21967350. DOI: 10.1002/ADMI.202201051. URL: https://www.researchgate.net/publication/364819692_Recent_Developments_of_Inkjet-Printed_Flexible_Energy_Storage_Devices.

[22] Marcel Lobos et al. "Manufactured microlenses by polimer inkjet printing". In: ().

[23] Daniil A. Lukyanov and Oleg V. Levin. "Inkjet Printing with (Semi)conductive Conjugated Polymers: A Review". In: *ChemEngineering 2024, Vol. 8, Page 53* 8.3 (May 2024), p. 53. ISSN: 2305-7084. DOI: 10.3390/CHEMENGINEERING8030053. URL: https://www.mdpi.com/2305-7084/8/3/53/htm%20https://www.mdpi.com/2305-7084/8/3/53.

[24] Hesam Maleki and Volfango Bertola. "Recent advances and prospects of inkjet printing in heterogeneous catalysis". In: *Catalysis Science and Technology* 10.10 (May 2020), pp. 3140–3159. ISSN: 20444761. DOI: 10.1039/D0CY00040J. URL: https://www.researchgate.net/publication/340675351_Recent_advances_and_prospects_of_inkjet_printing_in_heterogeneous_catalysis.

[25] Matti Mäntysalo et al. "Evaluation of inkjet technology for electronic packaging and system integration". In: *Proceedings - Electronic Components and Technology Conference* (2007), pp. 89–94. ISSN: 05695503. DOI: 10.1109/ECTC.2007.373781.

[26] *Manufacturing of the fully inkjet-printed dielectric elastomer actuator | TU Delft Repository*. URL: https://repository.tudelft.nl/record/uuid:a1750ba6-5d74-40a0-be9c-be965f8e0503.

[27] A. Menicanin et al. "Ink-jet printed CPW inductors in flexible technology". In: *2012 Proceedings of the 35th International Convention MIPRO* (2012).

[28] *Microsoft Word - UV-EB INKJET INKS_TB_04192019 | Enhanced Reader*.

[29] *mr-UVCur26SF*. 2019. URL: https://kayakuam.com/wp-content/uploads/2019/10/PI_mrUVCur26SF-1.pdf.

[30] *Nano Dimension Dielectric Ink 1092 - J.A.M.E.S*. URL: https://j-ames.com/ame-materials/nano-dimension-dielectric-ink-1092.

[31] *Nano Dimension Introduces Highly Conductive Silver Nanoparticle Inks*. URL: https://www.nano-di.com/newsroom/nano-dimension-introduces-agcite-highly-conductive-silver-nanoparticle-ink-for-printed-electronics.

[32] Praneet Pandey and Mohammad Taufik. "A Review on PolyJet 3-D Printing Process and Its Applications". In: *Lecture Notes in Mechanical Engineering* (2023), pp. 401–410. ISSN: 21954364. DOI: 10.1007/978-981-19-2188-9{_}37. URL: https://www.researchgate.net/publication/363397890_A_Review_on_PolyJet_3-D_Printing_Process_and_Its_Applications.

[33] Heung Yeol Park et al. "Control of surface wettability for inkjet printing by combining hydrophobic coating and plasma treatment". In: *Thin Solid Films* 546 (Nov. 2013), pp. 162–166. ISSN: 0040-6090. DOI: 10.1016/J.TSF.2013.03.067.

[34] *PolyJet Materials A Range of Possibilities*. URL: https://www.stratasys.com/contentassets/d8d320f3a1be4bac84ceb611b79e015b/wp_pj_polyjetmaterials_a4_0122a.pdf?v=49c18a.

[35] *Pre-treatment for printing and coating - Plasma applications*. URL: https://www.relyon-plasma.com/pretreatment-for-printing/?lang=en.

[36] Arivazhagan Pugalendhi, Rajesh Ranganathan, and Manivannan Chandrasekaran. “Effect of process parameters on mechanical properties of VeroBlue material and their optimal selection in PolyJet technology”. In: (). DOI: 10.1007/s00170-019-04782-z. URL: https://doi.org/10.1007/s00170-019-04782-z.

[37] Devin J. Roach et al. “The m4 3D printer: A multi-material multi-method additive manufacturing platform for future 3D printed structures”. In: *Additive Manufacturing* 29 (Oct. 2019), p. 100819. ISSN: 2214-8604. DOI: 10.1016/J.ADDMA.2019.100819.

[38] B. Salam and B. K. Lok. “Solderability and reliability of printed electronics”. In: *Proceedings of the International Symposium on the Physical and Failure Analysis of Integrated Circuits, IPFA* (2008). DOI: 10.1109/IPFA.2008.4588211.

[39] Ehab Saleh et al. “FULL PAPER 1700134 (1 of 8) 3D Inkjet Printing of Electronics Using UV Conversion”. In: (2017). DOI: 10.1002/admt.201700134. URL: https://doi.org/10.1002/admt.201700134..

[40] *Sci-Hub | Assembly of Components on Inkjet-Printed Silver Structures by Soldering. IEEE Transactions on Components, Packaging and Manufacturing Technology, 1–1 | 10.1109/tcpmt.2018.2855045*. URL: https://sci-hub.se/10.1109/tcpmt.2018.2855045.

[41] *Silver Nano List of Products | Mitsubishi Paper Mills*. URL: https://www.mpm.co.jp/electronic/eng/silver-nano/line-up.html.

[42] *Silver nanoparticle ink 30 wt dispersion in ethylene glycol Silver ink*. URL: https://www.sigmaaldrich.com/NL/en/product/aldrich/798738.

[43] *Silver nanoparticle ink 50 wt. , dispersion in tripropylene glycol mono methyl ether Silver ink*. URL: https://www.sigmaaldrich.com/NL/en/product/aldrich/796042.

[44] Dogan Sinar and George K. Knopf. “Cyclic Liquid-Phase Exfoliation of Electrically Conductive Graphene-Derivative Inks”. In: *IEEE Transactions on Nanotechnology* 17.5 (Sept. 2018), pp. 1020–1028. ISSN: 1536125X. DOI: 10.1109/TNANO.2018.2849264.

[45] Enrico Sowade et al. “Toward 3D-Printed Electronics: Inkjet-Printed Vertical Metal Wire Interconnects and Screen-Printed Batteries”. In: *Advanced Engineering Materials* 21.10 (Oct. 2019). ISSN: 15272648. DOI: 10.1002/ADEM.201900568.

[46] *Structural Electronics 2017-2027: Applications, Technologies, Forecasts*. URL: https://www.prnewswire.com/news-releases/structural-electronics-2017-2027-applications-technologies-forecasts-300505604.html.

[47] *The History of PCBs| Fineline Global*. URL: https://www.fineline-global.com/knowledge-centre/the-history-of-printed-circuit-boards-in-a-nutshell/.

[48] *Verbesserung der Präzision mittels Inkjet-Technologie | Über 3D-Drucker | Hersteller von leistungsfähigen 3D-Druckern KEYENCE [AGILISTA]*. URL: https://www.keyence.de/ss/products/3d-printer/agilista/3dprinter/inkjet/.

[49] *VisiJet M2S-HT250 High Temperature Plastic | 3D Systems*. URL: https://www.3dsystems.com/materials/visijet-m2s-ht250.

[50] Florens Wasserfall. *Embedding of SMD Populated Circuits into FDM Printed Objects*. 2015. URL: https://hdl.handle.net/2152/89317.

[51] Florens Wasserfall et al. “Topology-aware routing of 3D-printed circuits”. In: *Additive Manufacturing* 36 (Dec. 2020). ISSN: 22148604. DOI: 10.1016/J.ADDMA.2020.101523.

[52] *What Can You Print on With UV Flatbed Printers | Roland DG*. URL: https://www.rolanddg.eu/en/blog/2023/08/31/uv-flatbed-printers.

[53] *What is Drop On Demand?: Benefits, challenges and differences.* URL: https://www.ubscode.com/en-ww/news/150/que-es-el-drop-on-demand.

[54] Karl Willis. *Project Wire*. URL: https://www.karlddwillis.com/project-wire/.

A

Slicer main program loop

In this chapter, a more in-depth overview is given of the structure of the main slicing algorithm, visualized in Figure A.1.
To avoid excessive memory usage in the program, only one sliced layer is stored in memory at once, and thus the full volumetric data of the model is not accessible. In order to generate structures that span multiple layers, such as support structures or sliced circuits, persistent storage buffers are used to transfer information between layers. This, in combination with the slicing order, which is from top to bottom, makes it possible for the slicing algorithm to 'look up' at layers that are positioned above the current layer, but it is not possible to 'look down' as those layers have not been generated yet.

In the slicer, a variable is present which keeps track of the current layer index, called *i* in the diagram. This starts out as the total number of layers in the model, and decreases for each generated layer, until it reaches 0 when the slicing is finished.
For each layer, the model is sliced and rasterized at the current layer index, and this slice is stored as the structural layer. From this layer, cavities are removed in the case that vias or embedded components are present in the layer. The shapes of these cavities are defined as parametric 3D level-set functions, which allows for simple rectangular shapes for components, as well as more complex shapes for the vias, such as cones and ramps.

After this is performed, the structural layer is essentially finished and the circuit slicing is performed. The main purpose of the circuit slicing algorithm is to ensure that the maximum jetting height is not exceeded, by splitting circuits into segments. However, to determine when this is necessary, it must first be determined how the circuit layer is laid down on the structural layers, as this may not be uniform for the entire circuit layer.
As this is dependent on the 3D geometry of the model, storage buffers are used to carry information in-between layers. These are the following:

- ***circuit layer storage buffer*** : 2D buffer which stores segments of the circuit layers that have not been laid down yet
- ***circuit layer export buffer***: 2D buffer which stores segments of the circuit layers that have been laid down, but are not yet exported.
- ***j***: Integer value that keeps track how many layers more may be traversed before the jetting height is exceeded.
- ***circuit layer origin index***: Integer value that stores at which layer index the current *circuit layer export buffer* should be printed.

When the slicing algorithm encounters a layer where a circuit layer is present, the 2D circuit layer data is added to the *circuit layer storage buffer* by means of a logical or-operation. When this happens, *j* is set to 0, and *circuit layer origin index* is set to the current layer index. When the slicing algorithm now

continues slicing and traverses down the layers, *j* is decreased by 1 for each traversed layer. Additionally, it is checked if parts of the *circuit layer storage buffer* can be laid down on the current structural layer, through means of a logical and-operation. When this is the case, that section is removed from the *circuit layer storage buffer*, and added to the *circuit layer export buffer*.

When *j* reaches a value of 0, the entire *circuit layer export buffer* is converted to a bitmap image and exported as a file. The name of this file indicates the layer at which it should be printed, which is equal to the *circuit layer origin index*. Next, *j* is set to the maximum jetting height divided by the layer height, and *circuit layer origin index* is set to the index of the current layer.

In this way, it is ensured that when a new circuit layer is added to the *circuit layer storage buffer*, the *circuit layer export buffer* is cleared. This is required, as the new circuit layer may be embedded in structural material, and therefore the layer at which it is printed needs to be equal to the layer at which is present in the model.

When the bottom layer of the model is reached, and thus *i=0*, the entirety of the *circuit layer storage buffer* is added to the *circuit layer export buffer* and exported..

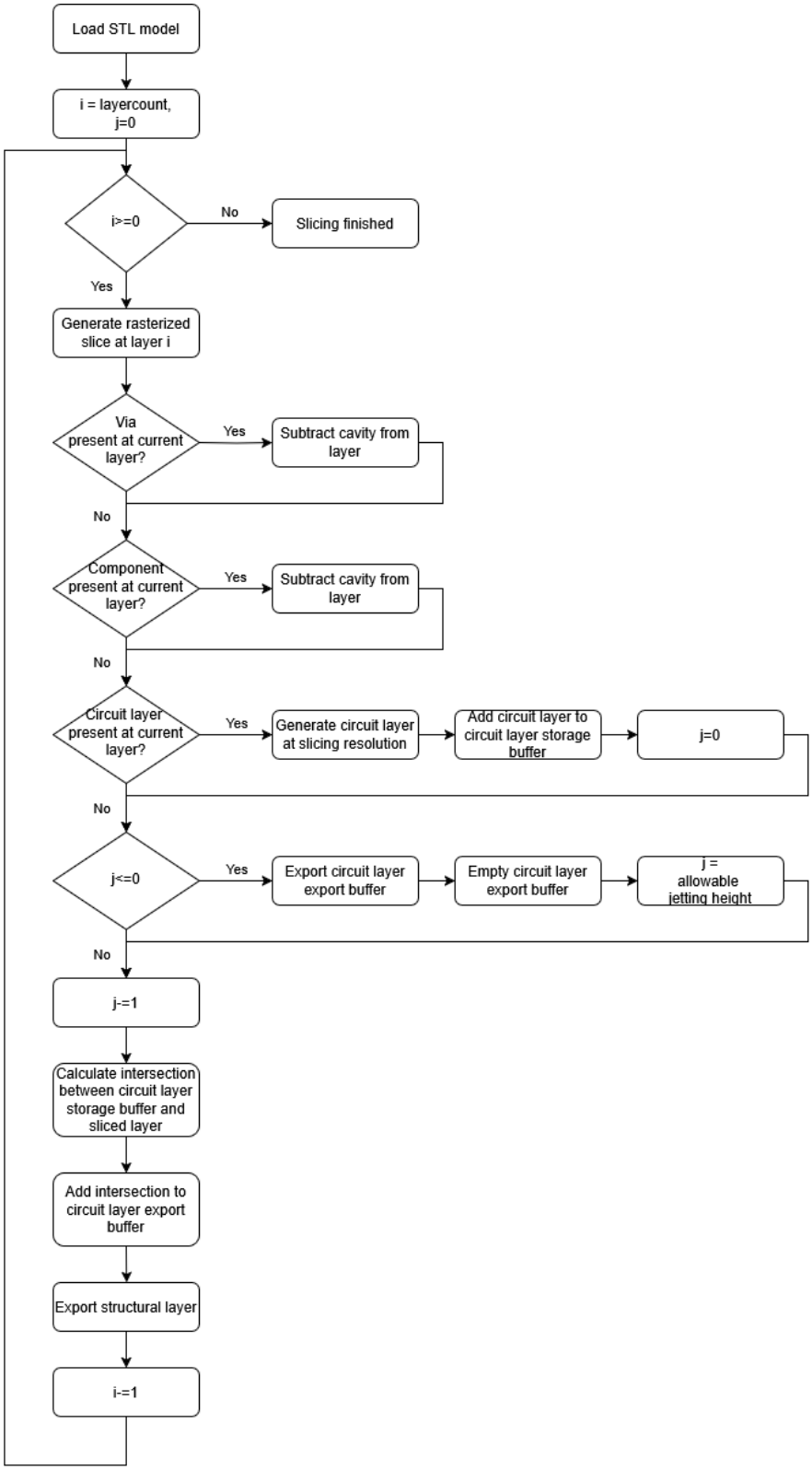


Figure A.1: Diagram of the functioning of the main slicing algorithm

B

Slicer documentation

The slicer developed in this thesis is released on github under the name SquidSlicer, and can be found at `https://github.com/MartijndenHoed/SquidSlicer`. An overview of the functions and UI of the program is given in the following section.

3D view mode

The default mode in the slicer is the 3D view. In this mode, STL models can be imported, sliced, and exported. In this mode, the controls are as follows:

- Drag left mouse button: Rotate the camera
- Drag middle mouse button: Move the camera
- Scroll + Ctrl: Zoom in/out
- Scroll: (In layer view) Move up/down through the sliced layers

In Figure B.1, a screenshot of the slicer can be seen where the elements have the following functions:

1. Import a STL model. In case no models have yet been imported, the loaded model represents the main structure. In case a model is already present, the newly imported model becomes a secondary structure.
2. Center the model in the middle of the build plate at zero height.
3. Slice the model at low resolution and generate a 3D preview of the bitmap stack.
4. Slice the model at high resolution and export the bitmap stack to a user-specified folder.
5. Edit the slicer settings.
6. Create a circuit layer. The user can choose to create a layer at the current height (the highest visible layer), or on the main structure (Which enables sandwich slicing). After creating the circuit, the circuit editing mode is activated. This function can only be used after a sliced preview of the model has been generated.
7. Open the circuit layer menu. Here, the user may edit or remove existing circuit layers.
8. Clear all present models and circuit layers.
9. Preview of the 3D model. Before slicing, the model is displayed as the STL mesh. After slicing, the model is displayed as a bitmap stack.
10. Representation of the printer buildplate, displayed as a $200x200mm$ square.

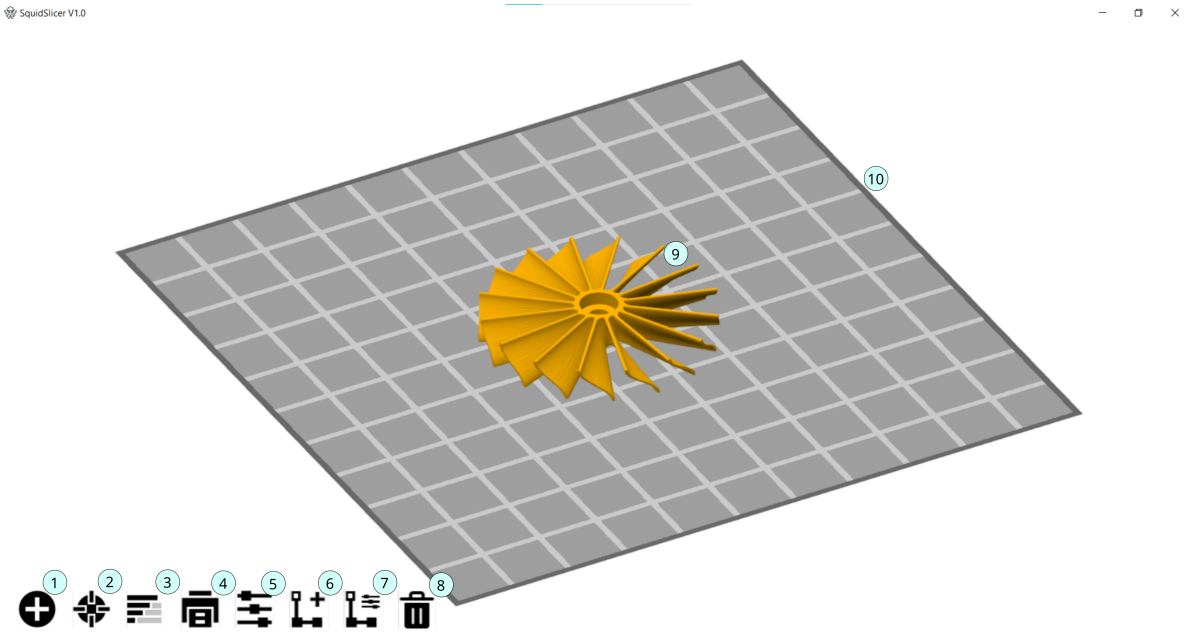


Figure B.1: Model preview of the developed slicer

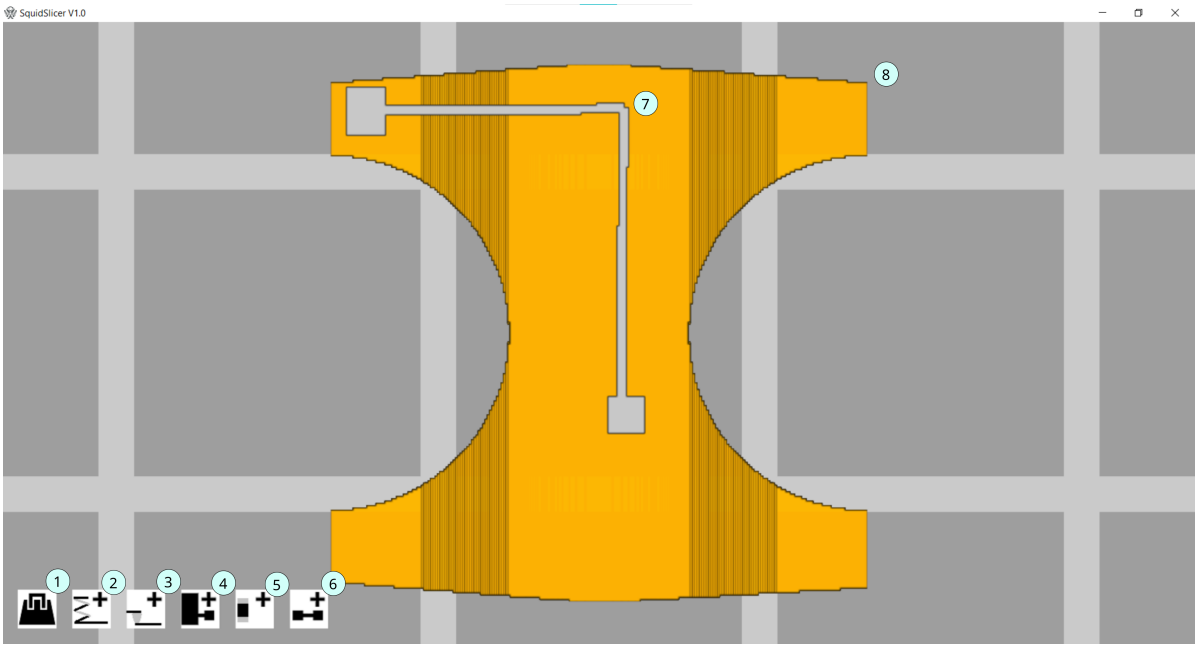


Figure B.2: Circuit editing mode in the developed slicer

Circuit editing mode

After creating a circuit layer, the circuit editing mode is opened. In this mode, the user can design circuits by drawing traces and pads, and add electronic components and elements. The camera rotation is locked to a top view of the model, but the user may still scroll through the sliced layers.
In Figure B.3, a screenshot of the slicer can be seen where the elements have the following functions:

1. Exit the circuit editing mode and return to the 3D preview.
2. Create a stairwell-via. After activating this function, clicking on the model generates a stairwell-via to a different user-specified circuit layer. Right-clicking an existing via removes it.
3. Create a dimple-via. After activating this function, clicking on the model generates a stairwell-via to a different user-specified circuit layer. Right-clicking an existing via removes it.
4. Draw a pad. After activating this function, clicking once on the model selects the first corner of the pad, clicking again selects the second corner and generates the pad. Right-clicking an existing pad removes the pad.
5. Add an electronic component. After activating this function, the user can select a component and specify the placement angle, after which it can be added to the model. Right-clicking an existing component removes it.
6. Draw a trace. After activating this function, clicking once on the model selects the first node of the trace, clicking again selects the second node and generates the trace. Right-clicking an existing trace removes it.
7. Preview of the circuit layer currently being worked on.
8. Top view of the sliced model at the current layer.

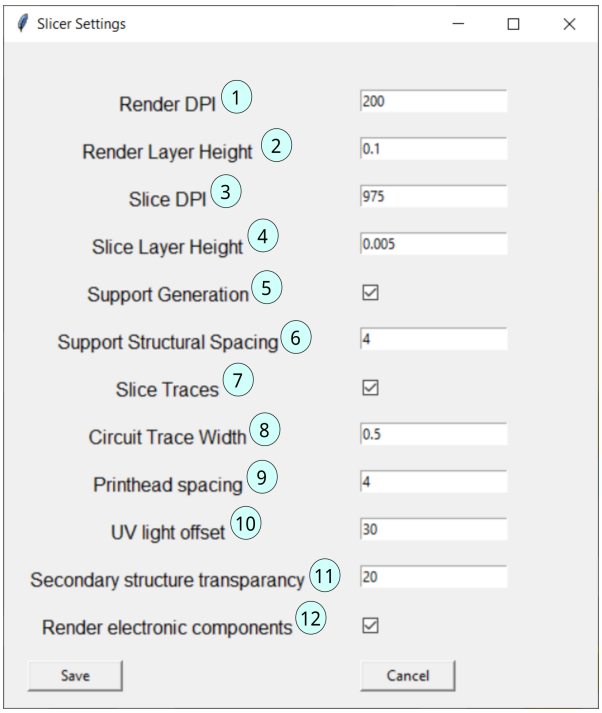


Figure B.3: Main slicer settings in the developed slicer

Slicer settings

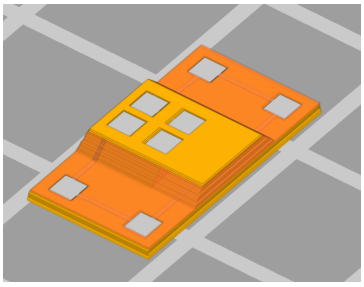
In Figure B.3, the settings and parameters which can be edited in the slicer can be seen. The explanation for these settings is as follows:

1. Resolution at which the 3D preview is sliced.
2. Layer height at which the 3D preview is sliced
3. Resolution at which the model is sliced upon exporting.
4. Layer height at which the model is sliced upon exporting.
5. Enable support generation for overhanging structures. This is not compatible with electronic circuits.
6. Specify the spacing between pillars of structural material in the support structure. A value of 0 means all support material consists of structural material, for higher values less structural material is integrated.
7. Enable the 3D slicing of circuit layers. If this mode is not enabled, circuit layers are rendered as 2D layer. If this mode is enabled, circuit layers are sliced and conform to the substrate upon which they are positioned.
8. The maximum distance between the printhead and the substrate in millimeter, also known as the maximum jetting height. When the height of a circuit layer exceeds this value, it is vertically split into segments.
9. Distance between the UV-light mounted on the printhead, and the nozzle array of the printhead. This adds a band of transparent pixels in exported bitmaps of structural layers to ensure that the UV light scans over the deposited material.
10. Transparency of secondary structures after slicing. Lower values allow the user to see embedded circuits in sandwich slicing mode.
11. Enable the rendering electronic components. If this setting is enabled, electronic components are rendered as black structures after slicing.

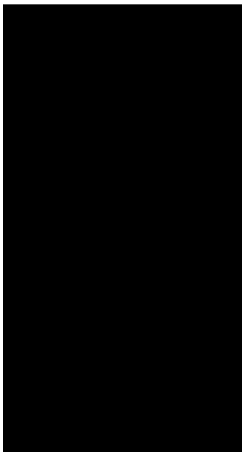
Exported files

Upon exporting, the user can specify a location and filename under which the sliced files are to be stored. A folder is created where the layers are then saved. 3 types of layers are currently supported when exporting, those being:

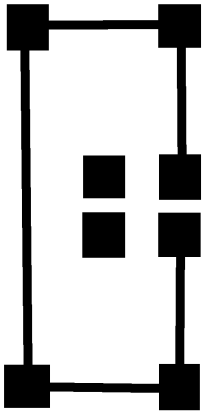
- Structural layers, saved in the format *struc_i.png*, where *i* represents the index of the layer at which it should be printed
- Circuit layers, saved in the format *circ_i.png*, where *i* represents the index of the layer at which it should be printed
- Structural fill layers, saved in the format *strucfill_i_j.png*. Here, i represents the index of the layer at which it should be printed, j represents the index of the fill layer. These layers represent the secondary structures in the sandwich slicing mode. These layers are printed sequentially without raising the printhead for each layer.



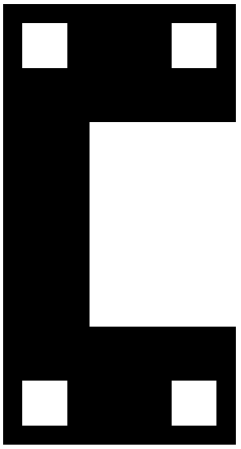
(a) Example of a model sliced in sandwich slicing mode



(b) First structural layer of the exported model, labeled *struc_0.png*



(c) Circuit layer of the exported model. It is printed on top of the main structure of the model, which has a height of 399 layers. Therefore, the layer is labeled as *circ_399.png*



(d) First layer of the strucfill (orange) layers of the model. It is printed on top of the main structure of the model, which has a height of 399 layers. Therefore, the layer is labeled as *strucfill_400_0.png*

Figure B.4: Example of a sliced model, with its layers displayed after exporting.

C

LP50 printing profile

Below, the profiles used for printing the TPGDA photoresin and AGNP ink can be found.

Table C.1: Printing profile used for printing the TPGDA photoresin

Setting	Value	Rationale
Active nozzles	All	Maximize print speed
Print repeats	1	Every layer is an individual image and is printed once
Print speed	150 mm/s	Reduce bleeding
Acceleration Y-axis	700 mm/s^2	Reduce bleeding
Scan direction	Bidirectional	Maximize print speed
Quality factor	1	Maximize print speed
Step size	12	Reduce nozzle artifacts
Droplet TOF	0.153	Z-offset/droplet velocity
Printhead Z-offset	0.5mm	Minimized to achieve better quality
DPI X-axis	975	(step size +1) * number of nozzles
DPI Y-axis	2000	Calibrated manually
Cure LED intensity	100%	A high intensity might help against oxygen inhibition, and has no real downside
Cure speed (normal)	20mm/s	Sufficient for curing, could be lowered
Cure speed (overcuring)	1mm/s	For reducing hydrophobicity of the TPGDA

Table C.2: Printing profile used for printing the NovaCentrix Metallon JS-A211

Parameter	Value	Rationale
Active nozzles	8	Use only the most reliable nozzle
Print repeats	1	Print only 1 layer at once
Print speed	150mm/s	Lowered for improved quality
Scan direction	Unidirectional	Longer prints but better quality
Quality factor	1	Only 1 nozzle used
Step Size	1	Only 1 nozzle used
Dropler TOF	0.153	Z-offset/droplet velocity
Printhead Z offset	0.5mm	May be raised. Values >4mm have been tested successfully
DPI axis	1100	Tuned manually
UV LED scan speed	0.05mm/s	Sufficient for sintering in one pass
Layer count	2,6	Dependent on desired conductivity/robustness. 2 was found sufficient for basic circuits, >5 is advised when soldering components

D

Additional test-prints

In This section, additional pictures of the fabricated test-prints are presented. These include:

- A repetition of the line test, with 2 additional bear-like models, to test the quality of curved geometries.
- A circuit ramp test, where the AGNP is printed on a set of ramps with varying slopes.
- An attempt to integrate a microcontroller and a more complex circuit into a structural component.



(a) Top view

(b) Angled view

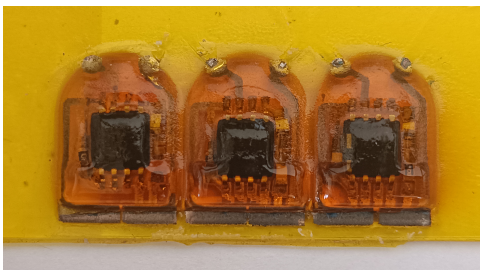
Figure D.1: Test-print containing lines with varying taper-angles and gummybear-like models.



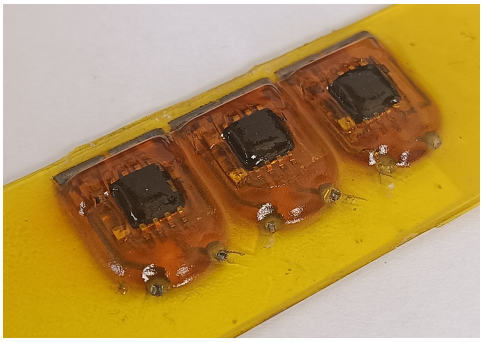
(a) Top view

(b) Angled view

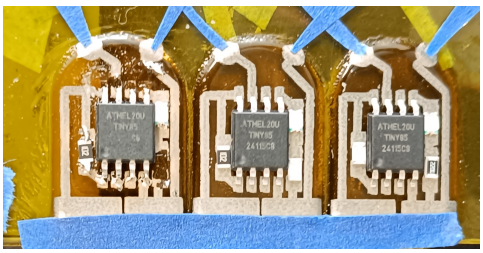
Figure D.2: Test-print of silver traces printed on slopes of varying angles.



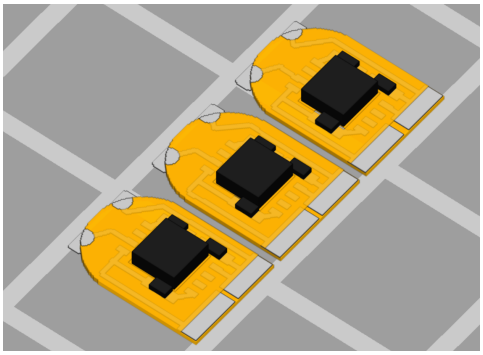
(a) Top view



(b) Angled view



(c) Top view during overprinting steps. Masking tape is added to cover pads.



(d) Section view of the model in the slicer, showing the embedded components as black rectangles.

Figure D.3: Test circuit with an embedded Attiny85 microprocessor. Print was aborted due to printer malfunction.